Nuclear Engineering and Design xxx (2009) xxx–xxx

Contents lists available at ScienceDirect

Nuclear Engineering and Design

journal homepage: www.elsevier.com/locate/nucengdes

Thermal hydraulic analysis for grid supported pressurized water reactor cores

C. Shuffler*, J. Trant, J. Malen, N. Todreas

Department of Nuclear Science and Engineering, Massachusetts Institute of Technology, 77 Massachusetts Avenue, Cambridge, MA 02139-4307, United States

ARTICLE INFO

Article history:
Received 31 July 2007
Received in revised form 4 June 2008
Accepted 27 December 2008
Available online xxx

ABSTRACT

This paper presents the methodology and results for thermal hydraulic analysis of grid supported pressurized water reactor cores using U(45% wt)–$ZrH_{1.6}$ hydride fuel in square arrays. The same methodology is applied to the design of UO_2 oxide fueled cores to provide a fair comparison of the achievable power between the two fuel types. Steady-state and transient design limits are considered. Steady-state limits include: fuel bundle pressure drop, departure from nucleate boiling ratio, fuel temperature (average for UO_2 and centerline/peak for U–$ZrH_{1.6}$), and fuel rod vibrations and wear. Transient limits are derived from consideration of the loss of flow and loss of coolant accidents, and an overpower transient.

In general, the thermal hydraulic performance of U–$ZrH_{1.6}$ and UO_2 fuels is very similar. Slight power differences exist between the two fuel types for designs limited by rod vibrations and wear, because these limits are fuel dependent. Large power increases are achievable for both fuels when compared to the reference core power output of 3800 MW_{th}. In general, these higher power designs have smaller rod diameters and larger pitch-to-diameter ratios than the reference core geometry. If the pressure drop across new core designs is limited to the pressure drop across the reference core, power increases of ~400 MW_{th} may be realized. If the primary coolant pumps and core internals could be designed to accommodate a core pressure drop equal to twice the reference core pressure drop, power increases of ~1000 MW_{th} may be feasible.

1. Introduction

This paper presents the results from a parametric thermal hydraulic analysis to investigate the potential benefits of U(45% wt)–$ZrH_{1.6}$ fuel use in pressurized water reactor (PWR) cores. A thorough discussion of U–$ZrH_{1.6}$ fuel can be found in Olander et al. (2009). The study's goal was evaluation of the maximum achievable power that can be safely sustained in U–$ZrH_{1.6}$ fueled cores constructed of traditional square array fuel assemblies with grid spacers subject to steady-state and transient design limits. A range of core geometries (i.e., combinations of rod diameter and pitch) were investigated. Steady-state design limits were placed on the minimum departure from nucleate boiling ratio (MDNBR), fuel bundle pressure drop, and fuel temperature. Additional limits were placed on rod vibration and wear. Limits for three transients were also applied. These transients included the loss of flow and loss of coolant accidents (LOFA and LOCA), and an overpower transient. To provide a benchmark for evaluating the thermal hydraulic performance of U–$ZrH_{1.6}$, the analysis was also performed for UO_2 fuel.

This paper is organized as follows: an overview of the parametric study approach is presented, including a discussion of the reference PWR core and the individual steady-state and transient limits applied to each core design. Results are then presented showing the maximum achievable power for a range of core designs subject to both steady-state and transient design limits. Conclusions are drawn from this analysis regarding the thermal hydraulic performance of U–$ZrH_{1.6}$ and UO_2 fuels, and their respective optimal (i.e., maximum power) designs.

2. Reference design parameters

2.1. Reference PWR

The reference core for the thermal hydraulic analysis is the South Texas Project, a 4 loop PWR designed by Westinghouse. It provides a set of fixed hardware dimensions and operating conditions that define boundaries for the thermal hydraulic analysis to ensure the feasibility of new designs (i.e., ensure that new designs can be integrated into existing PWRs). The reference core dimensions and operating conditions that are fixed in this analysis are listed in Table 1.

The reference core power is

$$Q_{ref} = 3800\,MW_{th}$$

* Corresponding author. Tel.: +1 617 253 5296.
E-mail addresses: cartershuffler@gmail.com (C. Shuffler), todreas@mit.edu (N. Todreas).

0029-5493/$ – see front matter © 2009 Elsevier B.V. All rights reserved.
doi:10.1016/j.nucengdes.2008.12.028

Table 1
Fixed core parameters for the thermal hydraulic analysis (Shuffler et al., 2006).

Parameter	Symbol	Value
Core radius	R_{core}	~1.83 m (72 in.)
Core enthalpy rise[a]	Δh	204 kJ/kg
Inlet temperature	T_{inlet}	294 °C (561.2 °F)
System pressure	P_{sat}	15.51 MPa (2250 psi)
Radial peak to average power[b]	$F_{q'}$	1.65
Axial peak to average power	$F_{q'axial}$	1.55

[a] The core enthalpy rise was fixed to protect the steam generators, which mandates that the hot leg temperature, after core outlet and bypass flow mixing, remains below 326.7 °C (620 °F).
[b] Radial peak to average power is the ratio of the hottest subchannel power to average subchannel power.

Table 2
Fixed fuel assembly parameters for the thermal hydraulic analysis (Shuffler et al., 2006).

Parameter	Symbol	Value
Number of grid spacers*	N_{grid}	10
Grid spacer thickness	t_{grid}	0.5 mm
Assembly length	$L_{assembly}$	4.599 m (181.1″)
Active fuel length	L_h	4.26 m (168″)

* Located at the following axial locations from the bottom of the fuel assembly (m): 0.00, 0.148, 0.529, 1.051, 1.573, 2.356, 2.878, 3.139, 3.661, 4.183.

2.2. Reference fuel assembly

Dimensions and properties of the reference core fuel assembly that are fixed in this analysis are provided in Table 2. It is recognized that the South Texas Project's 4.26 m active fuel length is uniquely 0.61 m longer than typical PWRs.

The reference fuel pins have cladding and gap thicknesses of 0.571 mm and 0.082 mm, respectively. The reference fuel rod outer diameter is D_{ref} = 9.5 mm and the pitch-to-diameter ratio is $(P/D)_{ref}$ = 1.326.

3. Design constraints—hydride and oxide fuels

This section presents the steady-state and transient thermal hydraulic constraints and limits applied to U–$ZrH_{1.6}$ and UO_2 fueled designs. Many constraints involve detailed assumptions and derivations, as provided in the Appendix.

3.1. Steady-state design constraints

The steady-state design constraints, summarized in Table 3, include: MDNBR, fuel bundle pressure drop, and fuel temperature. Additional limits were placed on rod vibrations and wear to preclude: fluid-elastic instability, vortex shedding lock-in, and excessive turbulence induced vibration in cross and axial flow. The latter two are manifested through physical limits on sliding and fretting wear at the cladding/grid support interface. The bases for these constraints, as well as the terminology in the table, will be defined later in this section.

Table 3
Summary of steady-state thermal hydraulic design constraints.

Design constraints for:	Constrained parameters	Design limit
Vortex-shedding lock-in	VSM_{lift}, VSM_{drag}[a]	>0.3
Fluid-elastic instability	FIM[b]	<1
Fretting wear	$\frac{Q_{fretting,new}}{Q_{fretting,ref}}$[c]	≤1
Sliding wear	$\frac{Q_{sliding,new}}{Q_{sliding,ref}}$	≤1
DNBR	MDNBR	>2.17
Pressure drop	ΔP	<0.20 MPa (29 psi) <0.414 MPa (60 psi)
Fuel temperature	$T_{centerline}$ – U–$ZrH_{1.6}$ $T_{average}$ – UO_2	<750 °C <1400 °C

[a] VSM = vortex shedding margin.
[b] FIM = fluid-elastic instability margin.
[c] Q = cumulative volume of material removed by wear.

3.1.1. MDNBR

Departure from nucleate boiling (DNB) occurs at the critical heat flux, which is a function of the geometry and operating conditions in the core. It is characterized by a sharp decline in the heat transfer coefficient at the coolant/cladding interface, as vapor blankets the fuel rod preventing fluid from reaching its outer surface. The result is an abrupt rise in the temperature of both the fuel and cladding, which can cause a cladding breach and also damage the fuel.

The performance metric for DNB is the MDNBR, which is the minimum ratio of the critical to actual heat fluxes in the core (DNBR will vary axially and radially within the core). In commercial design, significant margin exists in the MDNBR limit to account for transients, core anomalies (e.g., rod bow), process uncertainty (e.g., instrument error), and correlation uncertainty. While it is difficult to quantify the magnitude of each uncertainty, a reasonable MDNBR limit was obtained by calculating the reference core's MDNBR. This was accomplished via execution of the VIPRE code at the reference core geometry and operating conditions (i.e., D = 9.5 mm, P/D = 1.326 and 3800 MW_{th}). The Versatile Internals and Component Program for Reactors; EPRI (VIPRE) code was developed by the Electric Power Research Institute (EPRI) to aid in the thermal hydraulic modeling and design of light water reactor cores (Stewart, 1989). This approach ensures that all new designs demonstrate the same level of DNB margin as the reference core at steady-state conditions. VIPRE evaluation of the critical heat flux for this parametric study used the W-3L correlation, developed by Westinghouse. This correlation was chosen because the reference South Texas Project core is a Westinghouse design, and the W-3L can be applied over a large range of hydraulic diameters compared with the other critical heat flux correlations in VIPRE. The MDNBR limit calculated was ~2.17. Fig. 1 below shows the various allowances incorporated into the steady-state MDNBR limit. The Safety Analysis MDNBR Limit (1.55) will be discussed in greater detail in Section 3.2.

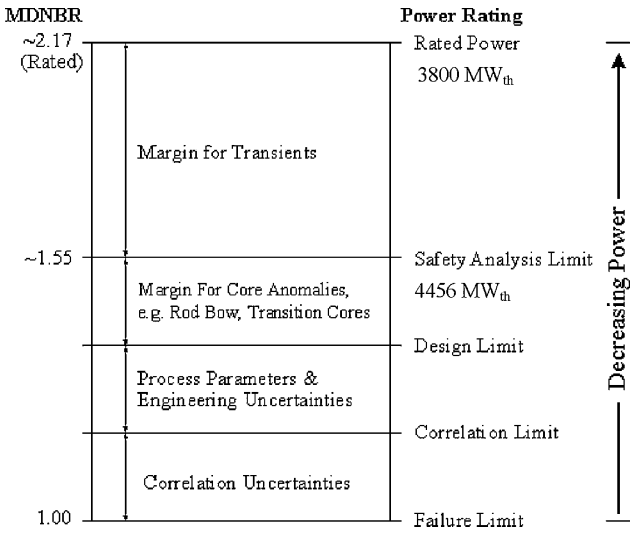

Fig. 1. Separated components of margin for MDNBR.

Please cite this article in press as: Shuffler, C., et al., Thermal hydraulic analysis for grid supported pressurized water reactor cores. Nucl. Eng. Des. (2009), doi:10.1016/j.nucengdes.2008.12.028

3.1.2. Pressure drop

The maximum pressure drop sustainable through the primary system is determined by the capability of the coolant pumps. Two separate pressure drop limits were used in the steady-state thermal hydraulic analysis to reflect the current and 5 year expected enhanced states of pumping technology. While losses occur throughout the entire primary coolant loop, the limit is based on the pressure drop across the fuel bundle, because it will vary most among the redesigned cores.

The lower pressure drop limit indicative of current PWR pumping capacity was determined in the same manner as the steady-state MDNBR limit: calculating the pressure drop across the fuel bundle given by VIPRE execution for the reference core geometry and operating conditions. This pressure drop is ~0.20 MPa. The enhanced pressure drop limit is based on examination of pumping capacities for the Westinghouse AP600 and AP1000 PWR designs, and a survey of industry experts. The pressure drop in the core nearly doubled between the design of the AP600 and AP1000, so it is reasonable to believe that in the next 5 years, which is well before a hydride fueled core could be deployed, the capability could again double. The enhanced fuel bundle pressure drop limit chosen is therefore approximately double that of the reference PWR, or 0.414 MPa.

3.1.3. Fuel temperature

Based on experience with hydride fuels used in TRIGA reactors, a steady-state fuel centerline temperature limit of 750 °C was chosen for this analysis (Olander et al., 2009).

Unlike hydride fuels, oxide fuels release non-negligible amounts of fission gas. If not limited, this gas can pressurize and even burst the fuel pin. Based on simplified empirical models of fuel performance data for oxide fuels, it is assumed the fission gas release fraction can be kept below 5% by limiting the average fuel temperature to 1400 °C. This is the UO_2 temperature limit adopted for this analysis. Note that this limit is more constraining than adopting a peak temperature limit of 2800 °C, which is the melting point for UO_2.

3.1.4. Vibrations and wear limits

Three primary types of flow-induced vibration are observed for cylindrical fuel elements subject to cross and axial flow: vortex-induced vibration, fluid-elastic instability, and turbulence-induced vibration in cross and axial flow. Vibration amplitudes associated with vortex shedding lock-in and fluid-elastic instability are generally very large, and can quickly cause severe damage to the fuel rod and its support structure. These mechanisms must be prevented by adequate design of the fuel assembly structure for the flow conditions in the core (i.e., using an appropriate number of grid supports and providing adequate stiffness to the fuel rod). Turbulence-induced vibration is generally of small amplitude and cannot be avoided. The principal design concern is therefore not the prevention of the vibration mechanism, but the limitation of resultant wear at the cladding/rod support interface. Limits for all mechanisms are discussed in this section. The Appendix provides a list of key assumptions made in the vibrations and wear analysis.

3.1.4.1. Vortex shedding lock-in. Cross-flow over cylindrical elements generates vortices that are shed alternately from one side of the structure to the other. This shedding produces an uneven pressure distribution around the rod, and resultant forces act on the structure in both the lift (perpendicular to the flow) and drag (parallel to the flow) directions. The force component in the lift direction has a frequency equal to the vortex shedding frequency, f_s, while the drag component has a frequency equal to twice the vortex shedding frequency.

When the vortex shedding frequencies are well separated from the natural frequency of the rod, only mild vibrations occur. When the shedding frequency in either the lift or drag direction approaches any of the rod's natural frequencies, a phenomenon called lock-in occurs. In this event, the shedding frequency assumes the natural frequency of the vibrating rod, causing larger resonance-type vibrations. This effect may cause immediate failure of the rod, or lead to premature wear. Because the shedding frequency may shift to the natural frequency of the rod, sufficient separation must exist between the two frequencies to preclude this resonant behavior.

The vortex shedding frequency is given by

$$f_s = S\frac{V_{\text{cross}}}{D} \tag{1}$$

where the Strouhal number, S, was found by Weaver and Fitzpatrick (Au-Yang, 2001) to depend on the P/D ratio and channel shape. For square arrays,

$$S = \frac{1}{2(P/D-1)} \tag{2}$$

Cross-flow velocities vary both radially and axially within the core, and are calculated by the VIPRE code. For conservatism, the cross-flow velocity input into Eq. (1) was the peak cross-flow velocity in the core determined by VIPRE calculations. To assess the susceptibility of new core designs to vortex-shedding lock-in, a vortex shedding margin (VSM) is defined in both the lift and drag directions. This margin indicates the separation distance between the rod and shedding frequencies. Au-Yang recommends that lock-in will be avoided as long as this margin is greater than or equal to 30%. The vortex shedding margins in the lift and drag directions are defined as

$$\text{VSM}_{\text{lift}} = \frac{|f_1 - f_s|}{f_s} \tag{3}$$

$$\text{VSM}_{\text{drag}} = \frac{|f_1 - 2f_s|}{2f_s} \tag{4}$$

where f_1 is fundamental frequency of the rod and the design limit to avoid vortex-shedding lock-in is

$$\text{VSM}_{\text{lift}} \text{ and } \text{VSM}_{\text{drag}} \geq 0.30 \tag{5}$$

3.1.4.2. Fluid-elastic instability. Fluid-elastic instability of a tube bundle occurs when the cross-flow velocity reaches the critical velocity, at which point the vibration response of the tubes suddenly increases uncontrollably and without bound. Unlike other vibration mechanisms, the instability of the tube and therefore its vibration amplitude continue to increase as the cross-flow velocity rises above the critical value.

A fluid-elastic instability margin (FIM) is defined to quantify a tube bundle's performance with regard to this mechanism. It is the ratio of the maximum effective cross-flow velocity in the hot assembly where cross-flow velocities are highest, V_{eff}, to the critical velocity for the bundle geometry, V_{critical}:

$$\text{FIM} = \frac{V_{\text{eff}}}{V_{\text{critical}}} \tag{6}$$

The FIM can be thought of as a safety margin: as long as the effective cross-flow velocity remains below the critical velocity (and hence the FIM remains below 1), fluid-elastic instability will not occur. The design limit is therefore

$$\text{FIM} < 1. \tag{7}$$

The Appendix provides the derivation of V_{eff} and V_{critical}.

Please cite this article in press as: Shuffler, C., et al., Thermal hydraulic analysis for grid supported pressurized water reactor cores. Nucl. Eng. Des. (2009), doi:10.1016/j.nucengdes.2008.12.028

Table 4
Summary of transient thermal hydraulic design constraints.

Transient	Constrained parameter	Design limit
LOCA	T_{peak} – U–$ZrH_{1.6}$	<1050 °C
	T_{peak} – UO_2	<2800 °C
	T_{peak} – Zircaloy	<1204 °C
LOFA	MDNBR	The MDNBR during LOFA coast down for the reference core
Overpower	MDNBR	The MDNBR during an 18% overpower transient for the reference core = 1.55

3.1.4.3. Turbulence induced vibration in cross and axial flow. Turbulence from cross and axial flows generate random pressure fluctuations around fuel rods, causing them to vibrate. The energy associated with the pressure fluctuations is distributed over a wide range of frequencies. Vibration occurs when the rod selects the portion of this energy that is closest to its natural frequency. Unlike fluid-elastic instability or vortex shedding lock-in, whose respective impacts can be minimized and even eliminated via adequate design of the fuel assembly, turbulence-induced vibrations cannot be avoided. Furthermore, no specific design limits are applicable because the vibration amplitudes accompanying turbulence are small. The principal design concern is therefore not the prevention of the mechanism but the limitation of resultant wear at the cladding/rod support interface over time.

Assessing the wear performance of new core designs requires knowledge of the rod response, or its displacement amplitude. Turbulent flows and the associated pressure distributions causing rod vibration, however, are random; it is therefore impossible to determine a detailed time history of the rod response. Instead, probabilistic methods are used to estimate the root mean square (RMS) response from both cross and axial flow turbulence. The total rod response, y_{rms}, is the summation of the cross and axial flow contributions ($y_{rms\text{-}cross} + y_{rms\text{-}axial}$), and becomes the primary input to the wear performance portion of the vibrations analysis. The equations for the cross and axial flow RMS rod responses are presented in the Appendix.

3.1.4.4. Wear due to flow-induced vibration. There are two wear mechanisms addressed in this study: fretting and sliding wear. Fretting wear is the most common wear mechanism, and historically the most costly flow-induced vibration problem in the nuclear industry. Fretting results from combined rubbing and impaction between the fuel rod grid support springs and the cladding surface. Sliding, or adhesive, wear occurs by the rubbing motion between the grid support springs and cladding surface (i.e., as in a fuel rod twirling inside of its support springs). It is often difficult to distinguish between these two wear types. Fretting wear is typically associated with smaller vibration amplitudes for gapped supports, where both wear and impact stress make contributions to material degradation. Sliding wear is typically associated with slightly larger vibration amplitudes, and results from the relative motion of two surfaces in continuous contact with one another.

Because specific design limits for wear are not readily available, this analysis estimated cumulative rod wear for new designs and limited it, if necessary, to the end of life cumulative wear calculated for the reference core's fuel pins. Calculating cumulative wear requires that both a wear rate and fuel lifetime be determined. Modeling the rate and accumulation of wear for nuclear fuel rods, however, is extremely complex. This analysis adopts simplified models for qualitatively assessing fretting and sliding wear rates (i.e., wear rate as a function of RMS rod response and fuel geometry) (Au-Yang, 2001). The equations for the fretting wear rate, $\dot{W}_{fretting}$, and sliding wear rate, $\dot{W}_{sliding}$, are presented in the Appendix.

In general, the cumulative wear for a new design, Q_{new}, is equal to the product of the wear rate and the total time the fuel spends in the core at power. The fuel lifetime is equal to the product of the cycle length, T_c, and the number of fuel batches. Because the number of fuel batches is fixed in new designs to that of the reference core, the general wear limit equation can be written in the following form:

$$\frac{Q_{new}}{Q_{ref}} = \frac{(\dot{W}_{new} T_{c,new})}{(\dot{W}_{ref} T_{c,ref})} \leq 1 \quad (8)$$

Calculating the time fuel spends in the core requires knowledge of not only the achievable power, but also the discharge burnup for the fuel. Separate neutronic (Ganda et al., 2009) and fuel performance (Romano et al., 2009) analyses were undertaken to derive the maximum achievable burnups for U–$ZrH_{1.6}$ and UO_2 fuels. The cycle lengths were then calculated for input into the vibrations analysis. For information on the achievable burnup studies and cycle lengths, refer to Shuffler et al. (2009). Because the achievable burnup from the neutronic analysis depends on the fuel enrichment, enrichments for U–$ZrH_{1.6}$ and UO_2 had to be chosen for the wear analysis. Burnup and energy generation from a core generally increases with enrichment. 12.5% enrichment is favored by economic considerations (Shuffler et al., 2009) and was selected for U–$ZrH_{1.6}$ fuel. 5% enrichment was chosen for UO_2 fuel because it is closest to typical commercial fuel enrichments. Ideally, the wear analysis would be performed for each fuel enrichment.

Note in Eq. (8) that the cumulative wear, due to its dependence on cycle length, depends on fuel burnup. The burnup, when limited by fuel performance constraints, depends on power. Multiple iterations were therefore required in application of the wear limits to ensure that the power dependent burnups converged to consistent values (Shuffler et al., 2009).

3.2. Transient design constraints

Table 4 summarizes the transients considered in this analysis, as well as their constrained parameters and design limits.

3.2.1. Overpower transient

The overpower transient is based on the 18% overpower limit determined for a rod bank withdrawal at power in the reference core's Final Safety Analysis Report (South Texas Project FSAR). Evaluation of this transient depends on maintaining the same margin with respect to DNB for new hydride and oxide fueled designs at the overpower condition as that of the reference core. The overpower MDNBR limit, however, is not known because it is held as proprietary information. According to the FSAR, the MDNBR for the South Texas Project during the overpower transient is achieved at 17.27% overpower, slightly below the 18% limit. An acceptable design limit was therefore obtained for the parametric transient analysis by evaluating the MDNBR output from VIPRE for the reference core at the overpower condition (i.e., at $1.1727 \times 3800 = 4456\ MW_{th}$). This value is 1.55, as shown in Fig. 1.

3.2.2. Loss of coolant accident (LOCA)

According to Title 10 of the Code of Federal Regulations, Section 50.46 (10CFR50.46), LOCA analysis involves consideration of numerous design metrics: peak cladding temperature, cladding interaction with water/steam, cladding oxidation, and maintaining

Please cite this article in press as: Shuffler, C., et al., Thermal hydraulic analysis for grid supported pressurized water reactor cores. Nucl. Eng. Des. (2009), doi:10.1016/j.nucengdes.2008.12.028

amenable cooling conditions in the core. Considering each of these individual design parameters was beyond the scope of this work. A simpler approach was taken for the LOCA analysis in which the time dependent fuel and cladding temperatures following initiation of the transient were calculated with RELAP and compared with their respective temperature limits. The LOCA temperature limit for U–$ZrH_{1.6}$ is 1050 °C, as reported by Garkisch and Petrovic (2003). At temperatures above 1050 °C, the hydride matrix converts to α phase (body centered cubic), and becomes brittle. The LOCA temperature limit for UO_2 is the fuel's melting temperature, 2800 °C. The LOCA temperature limit for the zircaloy cladding is 1204 °C, as defined in 10CFR50.46. Steady-state power was reduced for designs if either the fuel or cladding temperatures exceeded their respective limits during the LOCA.

3.2.3. Loss of flow accident (LOFA)

Following a LOFA, the coolant flow rate through the core rapidly decreases (i.e., coastdown). A scram is initiated and control rods are driven into the fuel assemblies to stop power production. There is a time lag of ~1.5 s between the initiation of the LOFA and the insertion of the rods. This causes the coolant temperature to rise sharply. The primary concern during a LOFA is DNB. Core design with respect to this transient was based on maintaining the same margin with respect to DNB as that of the reference core. This was accomplished by ensuring that the most limiting MDNBR for new designs was greater than or equal to the limiting MDNBR for the reference core during the LOFA.

4. Design methodology

This section presents the steady-state and transient design methodologies applied to both U–$ZrH_{1.6}$ and UO_2 fueled designs.

4.1. Design variables and assumptions

The primary design variables are the fuel rod outer diameter, D or D_{rod}, and pitch, P. The design space for this study includes geometries in the range:

$$6.5\,\text{mm} \le D_{rod} \le 12.5\,\text{mm} \quad 1.074 \le \frac{P}{D} \le 1.54$$

Four hundred discrete geometries are evaluated within this space and are thought to bound the range of feasible designs that could be retrofitted in the reference PWR vessel. The number of rods per assembly and the layout of assemblies within the core are optimized to maximum the number of rods in the core based on a methodology developed at MIT (Malen et al., 2004). The position of control rods is variable, though their placement is patterned after the reference core.

4.1.1. Placement of fuel assemblies in the core

The number of fuel rods that can fit into the reference PWR vessel depends on the rod pitch, rod diameter, and, since partial fuel assemblies are not feasible, the number of fuel rods per fuel assembly, n minus the number of control fingers. Geometrically, it is unfavorable to fit square assemblies into a circular core because there will always be unused space at the periphery. An optimization technique is therefore employed to place the largest number of rods possible into the core without significantly exceeding its dimensions.

A hypothetical core arrangement is shown in Fig. 2 for a 1/8th core section. Due to symmetry, a 1/8th core section is adequate to model the full core. The dimension that is perpendicular to the fuel assemblies, $D_{core\text{-}perp}$, is slightly shorter than the dimension cut diagonally across the assemblies, $D_{core\text{-}diag}$, in order to provide space for the downcomer. The number of rows of assemblies that

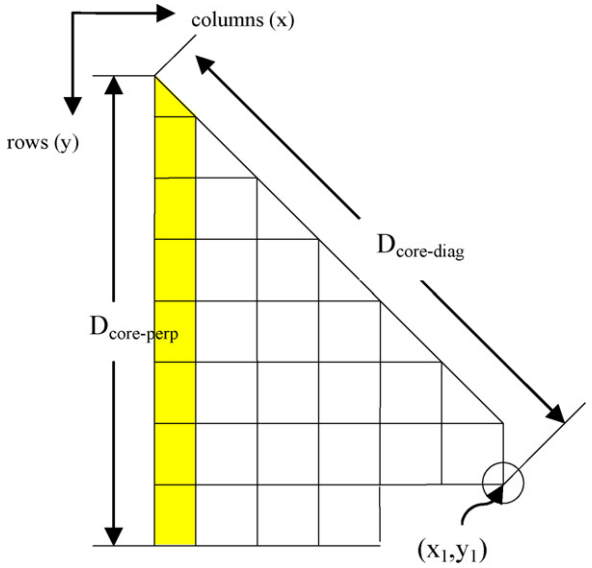

Fig. 2. Hypothetical fuel assembly arrangement for 1/8th core model.

can fit into the leftmost column in the figure is a function of the length of the assembly side, l_{assm}:

$$rows = \frac{D_{core\text{-}perp}}{l_{assm}} = \frac{D_{core\text{-}perp}}{\sqrt{n}P} \tag{9}$$

To minimize the wasted space at the core's outer periphery, the number of fuel rods per assembly is chosen by minimizing the following expression:

$$\min \left| \left(\frac{D_{ref\text{-}core}}{P\sqrt{n}} \right) - \text{round} \left(\frac{D_{ref\text{-}core}}{P\sqrt{n}} \right) \right|$$

$$\text{for} \sqrt{n} = [15,\ 16,\ 17,\ 18,\ 19,\ 20] \tag{10}$$

With n, D, and P defined, *rows* is determined by rounding the results from Eq. (9) to the nearest integer. Assemblies are stacked outward from this central column for each row until the dimension $D_{core\text{-}diag}$ is exceeded.

4.1.2. Placement of fuel rods in the fuel assembly

Rods are placed in fuel assemblies starting with the central position. If n is odd, as determined from the optimization algorithm in Eq. (10), a control rod is placed in the central position and at every third position outward. If n is even, the center of the assembly is a coolant channel, and control rods are placed equidistant from one another in the center of the assembly separated by two fuel rods on each side. The layouts for even and odd fuel assemblies are shown in Figs. 3 and 4. The central coolant channel for an even assembly is represented by the 1/8th coolant subchannel section numbered 1 in Fig. 3. The central control rod for an odd assembly is represented by the top control rod in Fig. 4.

4.1.3. Fuel rod properties

The fuel cladding is zircaloy for both U–$ZrH_{1.6}$ and UO_2 fuels. A liquid metal fill is applied in the gap between the fuel and cladding to enhance heat transfer, maintaining lower fuel temperatures. The liquid metal is a lead-bismuth-tin eutectic, in which each component is present at the same weight percentage. Helium was replaced by liquid metal for two reasons:

- Liquid metal has a thermal conductivity about 100 times higher than helium. The increased heat transfer coefficient across the gap prevents the fuel from reaching an excessive temperature thereby

Please cite this article in press as: Shuffler, C., et al., Thermal hydraulic analysis for grid supported pressurized water reactor cores. Nucl. Eng. Des. (2009), doi:10.1016/j.nucengdes.2008.12.028

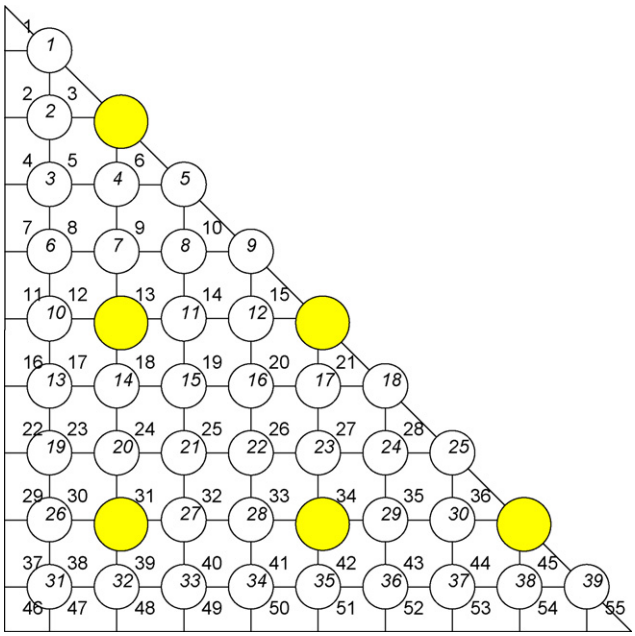

Fig. 3. Layout for an even fuel assembly.

limiting: fission gas release, hydrogen release (from U–$ZrH_{1.6}$), and irradiation induced fuel swelling.
- In the case of hydrogen release from the U–$ZrH_{1.6}$ fuel, liquid metal creates a barrier to prevent its diffusion into the cladding.

The properties of hydride fuel and consideration of the liquid metal bond are specifically addressed in Olander et al. (2009). In order to maintain consistency in the steady-state thermal hydraulic analysis, and not provide an unfair advantage to hydride fuels, liquid metal fill is also applied to the thermal hydraulic evaluation of UO_2 fuels. (For the LOCA analysis discussed in Section 5.3, oxide fuel is analyzed with helium fill, as is the reference core).

The following correlations for cladding and gap thickness were adopted for geometries in the parametric study that differ from the reference core geometry. These correlations are based on recommendations from industry experts.

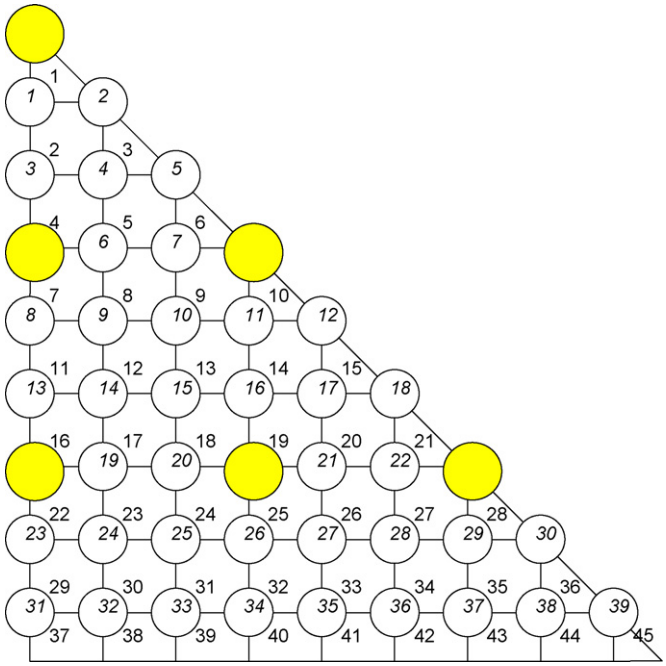

Fig. 4. Layout for an odd fuel assembly.

$$\text{If } D_{\text{rod}} < 7.747\,\text{mm} \tag{11}$$

$$t_{\text{clad}} = 0.508\,\text{mm}$$
$$t_{\text{g}} = 0.0635\,\text{mm}$$

$$\text{If } D_{\text{rod}} > 7.747\,\text{mm} \tag{12}$$

$$t_{\text{clad}} = 0.508 + 0.0362(D - 7.747)\,\text{mm}$$
$$t_{\text{g}} = 0.0635 + 0.0108(D - 7.747)\,\text{mm}$$

The correlations in Eqs. (11) and (12) were applied to both U–$ZrH_{1.6}$ and UO_2 fuels. It is recognized, however, that the increased swelling of hydride fuel relative to oxide fuel suggests a strong dependence of gap thickness on fuel burnup. This would increase the required initial gap thickness for hydride fuel rods. Though this effect was not included, the results presented in this study for hydride fuel would not be impacted because the high thermal conductivity of the liquid metal fill provides very little resistance to heat transfer across the gap.

4.2. Steady-state design methodology

Thermal hydraulic design accounting for the steady-state constraints presented in Section 3.1 adopts a methodology previously developed at MIT (Malen, 2003). This method linked the VIPRE sub-channel analysis code to a series of student-written MATLAB scripts to iteratively determine the maximum power for a range of user supplied geometries subject to thermal hydraulic design limits. The scripts automatically generate VIPRE input decks for a specified hydride/oxide geometry and assumed power, execute VIPRE, and extract relevant VIPRE output (e.g., MDNBR, pressure drop) for comparison with the applicable design limits. If no design limits are exceeded, the scripts execute VIPRE again with a higher power (or for a lower power if limits are exceeded). This iterative cycle continues until the maximum power is achieved. The process then repeats for the next geometry considered in the parametric study.

4.3. Transient design methodology

The transient thermal hydraulic investigation takes the output from the steady-state analysis as the initial condition, and evaluates the performance of new hydride and oxide fueled designs in the course of three transients: a LOCA, a LOFA, and an overpower event. The core power is reduced if the new design does not meet the transient design constraints defined in Section 3.2. The metric for determining transient performance is the MDNBR for the overpower and LOFA events, and cladding and fuel temperatures for the LOCA event. For the LOFA and overpower cases, the transients are initially applied to the reference core to determine the limiting MDNBR. The LOCA temperature limits were previously defined in Section 3.2. The three transients are then applied to U–$ZrH_{1.6}$ and UO_2 fueled designs, as determined by the steady-state thermal hydraulic analysis, to determine if either the MDNBR or cladding or fuel temperature limits are exceeded.

The overpower MDNBR was evaluated using the VIPRE code. The LOFA and LOCA analyses are more involved because they require the ability to determine time dependent conditions in the core during the transients, and the resulting MDNBR for the LOFA and the fuel and cladding temperatures for the LOCA. The RELAP code was used to evaluate the time dependent power and flow conditions in new designs and the reference core for the LOFA. This information was input into VIPRE to derive the time dependent MDNBR during the transient. The lowest MDNBR during the transient for new

Please cite this article in press as: Shuffler, C., et al., Thermal hydraulic analysis for grid supported pressurized water reactor cores. Nucl. Eng. Des. (2009), doi:10.1016/j.nucengdes.2008.12.028

designs had to remain above the lowest MDNBR for the reference core. If the limit was exceeded, the initial power was reduced. The RELAP code was also used to calculate the time dependent fuel and cladding temperatures for the LOCA. The Initial power provided by the steady-state analysis was reduced if either temperature limit was exceeded.

Unlike the steady-state thermal hydraulic analysis, MATLAB scripts were not developed to automate RELAP code execution. Evaluating the LOFA and LOCA transients for all geometries considered in the parametric study was therefore not possible, given project time constraints. Instead, the LOFA and LOCA transients were applied to select high power geometries of interest from the steady-state analysis (i.e., the peak power geometries incorporating the design limits from Table 3).

Additional transients could have been evaluated. Examples include a steam-line break with a stuck control rod and a control rod ejection accident. The three main transients included in this study, however, were considered to be the most limiting on achievable power.

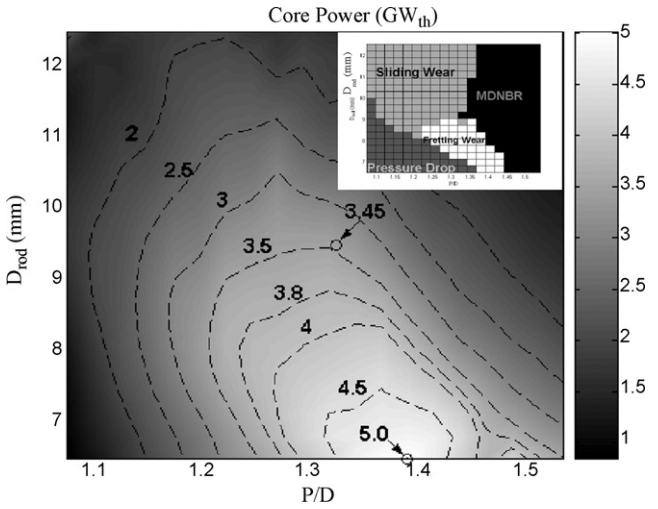

Fig. 5. Maximum power for 12.5% U–ZrH$_{1.6}$ incorporating steady-state design and overpower transient design limits at 0.414 MPa.

5. Results

This section presents the maximum achievable power results for both 12.5% enriched U–ZrH$_{1.6}$ and 5% enriched UO$_2$ incorporating both steady-state and transient design limits. Recall that some of these results may be enrichment dependent, because the wear limits are based on the time the fuel spends in the core which is partly a function of the neutronically achievable burnup. Results are presented separately for each pressure drop limit. As described in Section 4.3, the LOFA and LOCA analyses were applied to select geometries only. The thermal hydraulic results incorporating all limits except the LOFA and LOCA are therefore presented first in Sections 5.1 and 5.2. The LOCA and LOFA results are presented separately in Sections 5.3 and 5.4.

Results are presented on contour plots as a function of rod diameter and *P*/*D* ratio. For the four main cases evaluated in this study (e.g., hydride fuel at 0.414 MPa and 0.20 MPa, oxide fuel at 0.414 MPa and 0.20 MPa), a series of contour plots is provided. They include: (1) achievable power; (2) power, linear power, and rod number ratios; and (3) thermal hydraulic constraints. Each contour plot includes a vertical colorbar on the right side functioning as the key to map numerical values adjacent to the colorbar to the shading in the figure. Contour lines are also drawn on the figures to help the reader decipher the approximate numerical results.

5.1. Maximum achievable power results, 0.414 MPa pressure drop limit (no LOCA and LOFA)

The maximum achievable power subject to the steady-state, vibrations, and wear design limits discussed in Section 3.1 and the overpower transient design limit discussed in Section 3.2 is presented below for the 0.414 MPa pressure drop limit. Results include

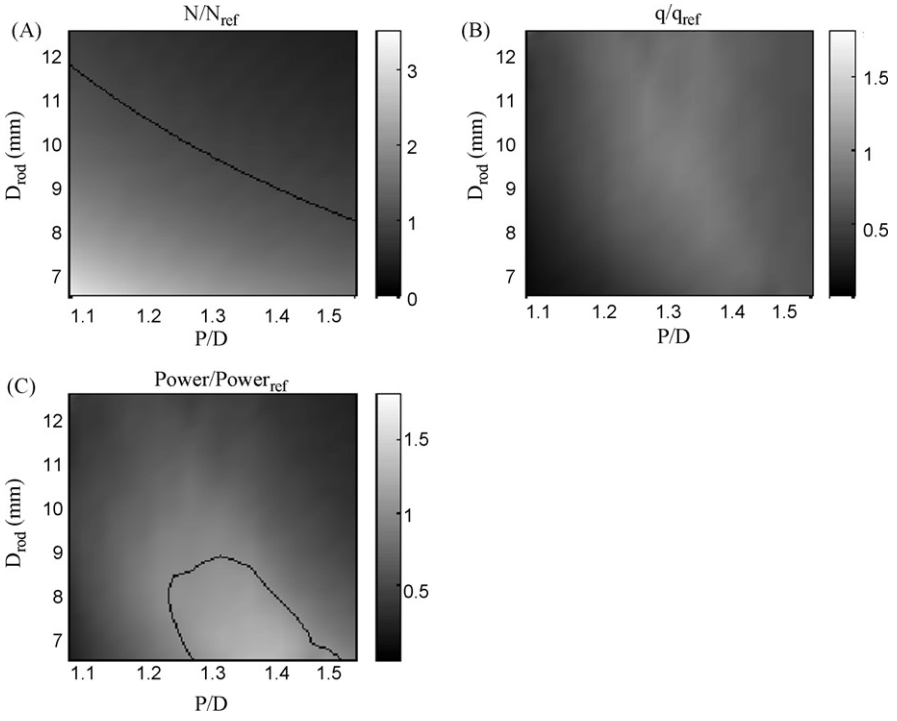

Fig. 6. Rod number, linear heat rate, and power ratios for 12.5% U–ZrH$_{1.6}$ at 0.414 MPa.

Please cite this article in press as: Shuffler, C., et al., Thermal hydraulic analysis for grid supported pressurized water reactor cores. Nucl. Eng. Des. (2009), doi:10.1016/j.nucengdes.2008.12.028

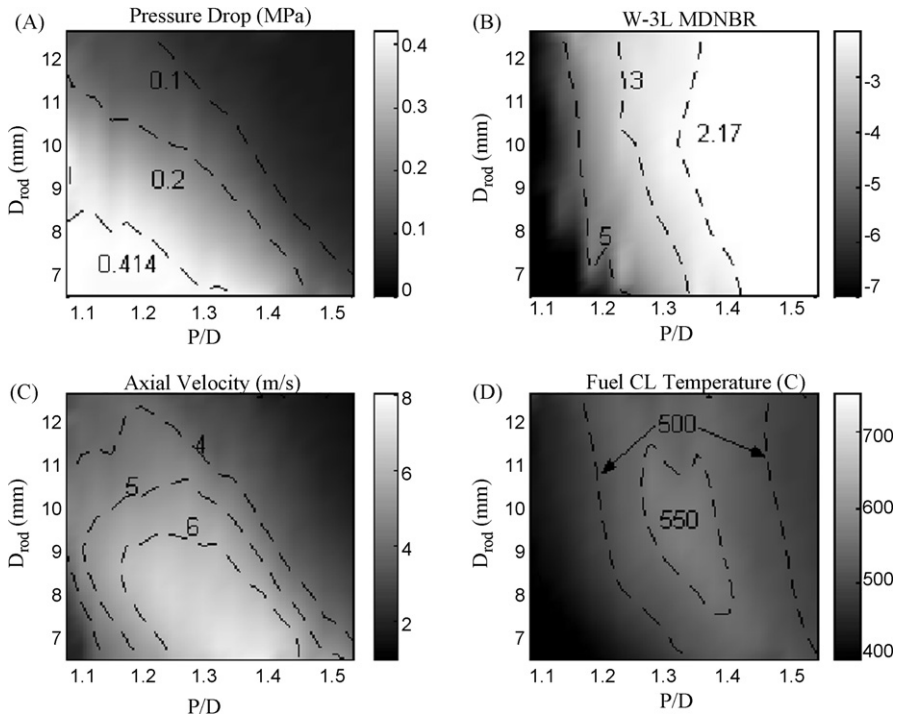

Fig. 7. Steady-state constraints for 12.5% U–$ZrH_{1.6}$ at 0.414 MPa.

plots of maximum power, and the steady-state and overpower transient constraints. The fluid-elastic instability margins were found to be very low (<0.1), and the steady-state MDNBR limit was always more constraining on achievable power than the transient overpower MDNBR limit. Hence, these two constraints are not plotted.

5.1.1. U–$ZrH_{1.6}$ results at 0.414 MPa

The maximum achievable power at the higher pressure drop limit is presented in Fig. 5 for 12.5% enriched U–$ZrH_{1.6}$ subject to all thermal hydraulic design limits except the LOFA MDNBR and LOCA temperature limits. The achievable power is the product of the average linear heat rate, as determined by VIPRE, and the number of fuel rods in the core. The power variations in Fig. 5 arise from changes in the average linear heat rate and rod number relative to the reference core values. Fig. 6 plots the ratios of the rod number, average linear heat rate, and power for the new geometries to the reference core's rod number, average linear heat rate, and power. A black line is used to denote the contour where each

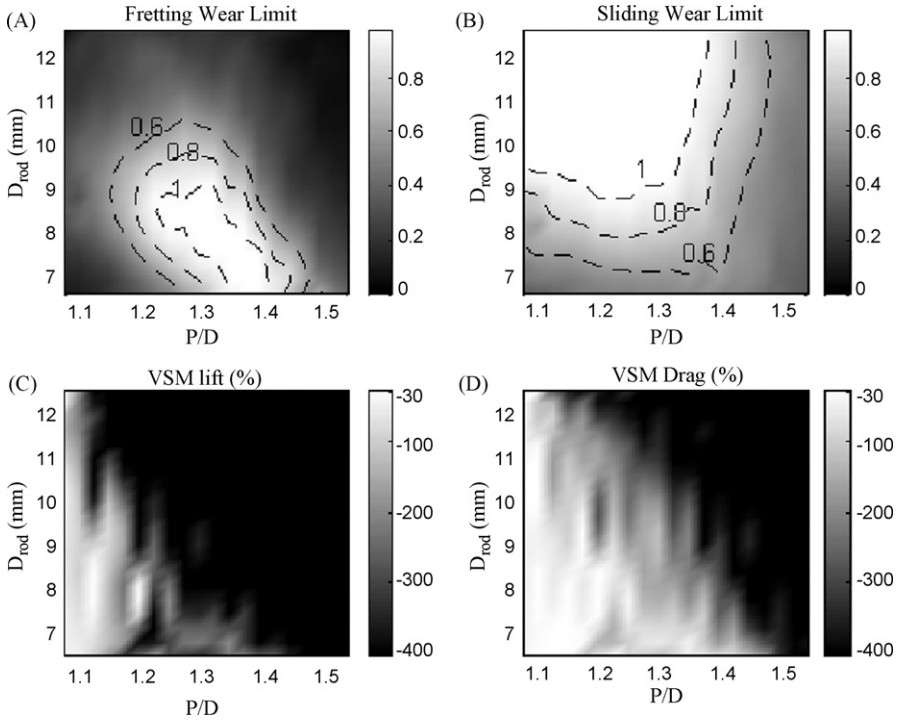

Fig. 8. Vibrations and wear constraints for 12.5% U–$ZrH_{1.6}$ at 0.414 MPa.

Please cite this article in press as: Shuffler, C., et al., Thermal hydraulic analysis for grid supported pressurized water reactor cores. Nucl. Eng. Des. (2009), doi:10.1016/j.nucengdes.2008.12.028

ratio is unity. Fig. 6A shows that approximately half of the design space in the parametric analysis has a higher rod number than the reference core. The most limiting constraints (i.e., the constraints that ultimately determine maximum power) are shown in the top right corner of Fig. 5. The numerical values for all constraints, both limiting and non-limiting, are plotted in Figs. 7 and 8.

The maximum power is 5.016 GW_{th}, or ~32% higher than the reference core power, and is achieved at the geometry: D_{rod} = 6.5 mm, P/D = 1.39. The limiting constraint is fretting wear. A large region exists inside of the reference power contour as shown in Figs. 5 and 6C that offer increased power relative to the reference PWR. Fig. 6A and B shows that these power gains result from increasing the number of fuel rods in the core. No geometries offer a higher average linear heat rate than the reference core. The power for the reference core geometry is 3.453 GW_{th}, or ~9% lower than the reference core power achieved at the reference core pressure drop 0.20 MPa. The reason for this reduction with hydride fuel is discussed in Section 6. MDNBR dominates as the most limiting constraint for larger P/D ratios. Pressure drop dominates for smaller rod diameters and smaller P/D ratios, while sliding wear dominates for larger rod diameters and larger P/D ratios. Fretting wear is the most limiting constraint for the highest power geometries. Fuel temperature, fluid-elastic instability, vortex shedding lock-in, and the overpower MDNBR do not constrain power for any geometry.

5.1.2. UO_2 results at 0.414 MPa

The maximum achievable power at the higher pressure drop limit is presented in Fig. 9 for 5% enriched UO_2. The power variations in Fig. 9 arise from changes in the average linear heat rate and rod number relative to the reference core values. Fig. 10 plots the ratios of the rod number, average linear heat rate, and power for the new geometries to the reference core's rod number, average linear heat rate, and power. The design constraints are plotted in Figs. 11 and 12.

The maximum power is 5.0 GW_{th}, or ~32% higher than the reference core power, and is achieved at the geometry: D_{rod} = 6.5 mm, P/D = 1.39. Like U–$ZrH_{1.6}$, the maximum power geometry at the higher pressure drop limit is constrained by the fretting wear limit. A large region exists inside of the reference power contour (i.e., 3.8 GW_{th}) shown in Figs. 9 and 10C indicating designs that offer increased power relative to the reference PWR. Fig. 10 shows that this region of increased power results from increased rod number. Though Fig. 10B shows that a portion of the design space offers a higher average linear heat rate than the reference PWR, the smaller number of fuel rods for these geometries offsets this gain. The result is that the final power in this region is lower than the reference PWR's power. The power at the reference core geometry is 3.8 GW_{th}. Power is limited by MDNBR, sliding wear, fretting wear, and pressure drop, as shown in the constraint subplot in Fig. 9.

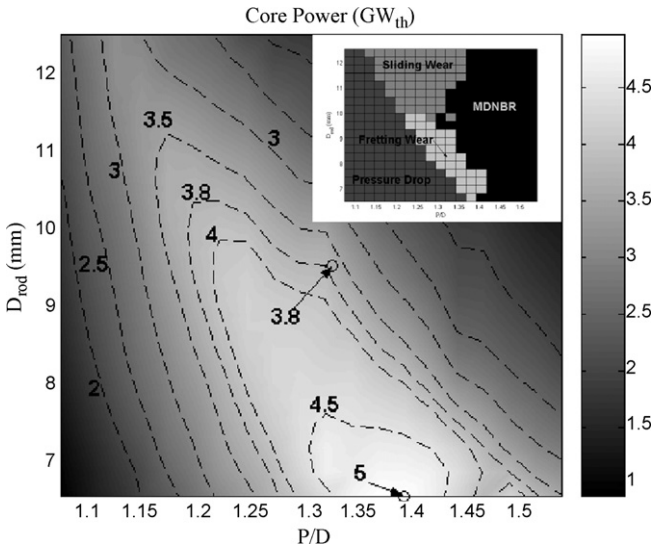

Fig. 9. Maximum power for 5% UO_2 incorporating steady-state and overpower transient design limits at 0.414 MPa.

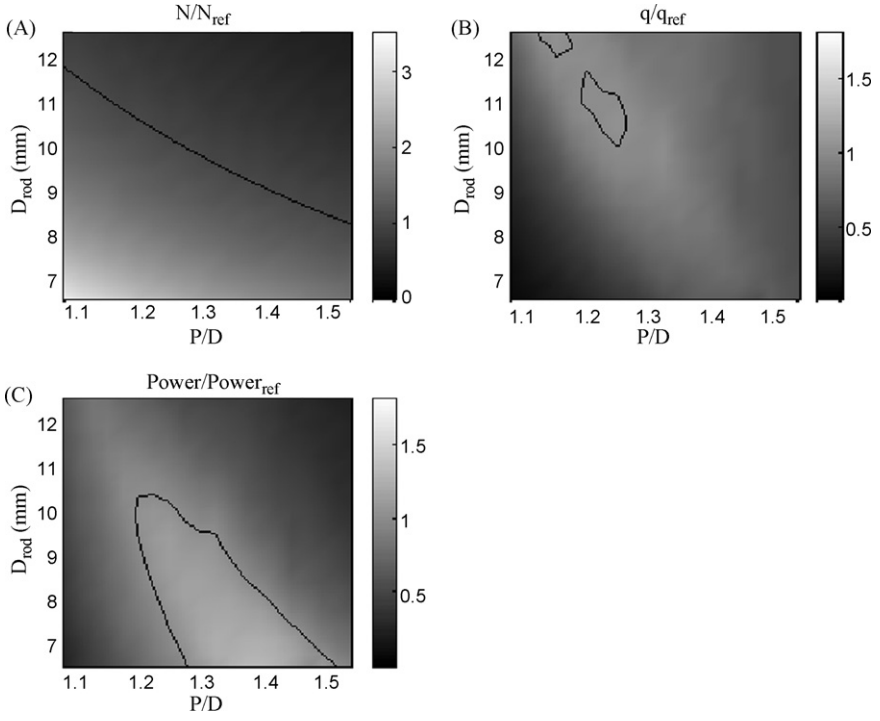

Fig. 10. Rod number, linear heat rate, and power ratios for 5% UO_2 at 0.414 MPa.

Please cite this article in press as: Shuffler, C., et al., Thermal hydraulic analysis for grid supported pressurized water reactor cores. Nucl. Eng. Des. (2009), doi:10.1016/j.nucengdes.2008.12.028

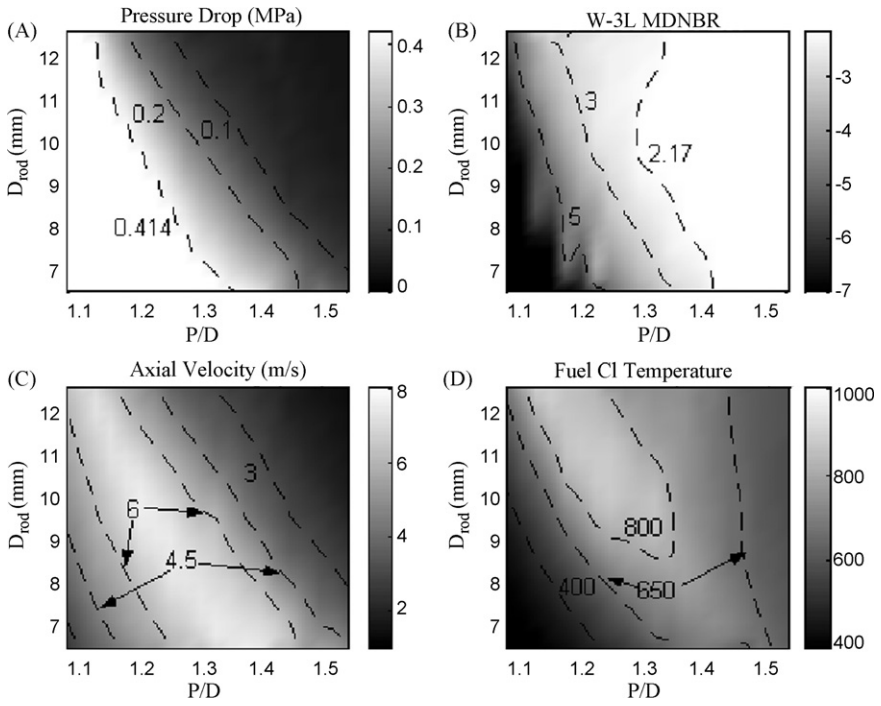

Fig. 11. Steady-state constraints for 5% UO_2 at 0.414 MPa.

5.2. *Maximum achievable power results, 0.20 MPa pressure drop limit (no LOCA and LOFA)*

The maximum achievable power subject to the steady-state, vibrations, and wear design limits discussed in Section 3.1 and the overpower transient design limit discussed in Section 3.2 is presented below for the 0.20 MPa pressure drop limit. Results include plots of maximum power, and the steady-state and overpower transient constraints. Like the 0.414 MPa case, the fluid-elastic instability margins were found to be very low (<0.1), and the overpower transient MDNBR was never as limiting on power as the steady-state MDNBR. Hence, these margins and MDNBR values are not plotted.

5.2.1. *U–$ZrH_{1.6}$ results at 0.20 MPa*

The maximum achievable power at the reference core pressure drop limit is presented in Fig. 13 for 12.5% enriched U–$ZrH_{1.6}$. The power variations in Fig. 13 arise from changes in the average linear heat rate and rod number relative to the reference core values. Fig. 14 plots the ratios of the rod number, average linear heat rate,

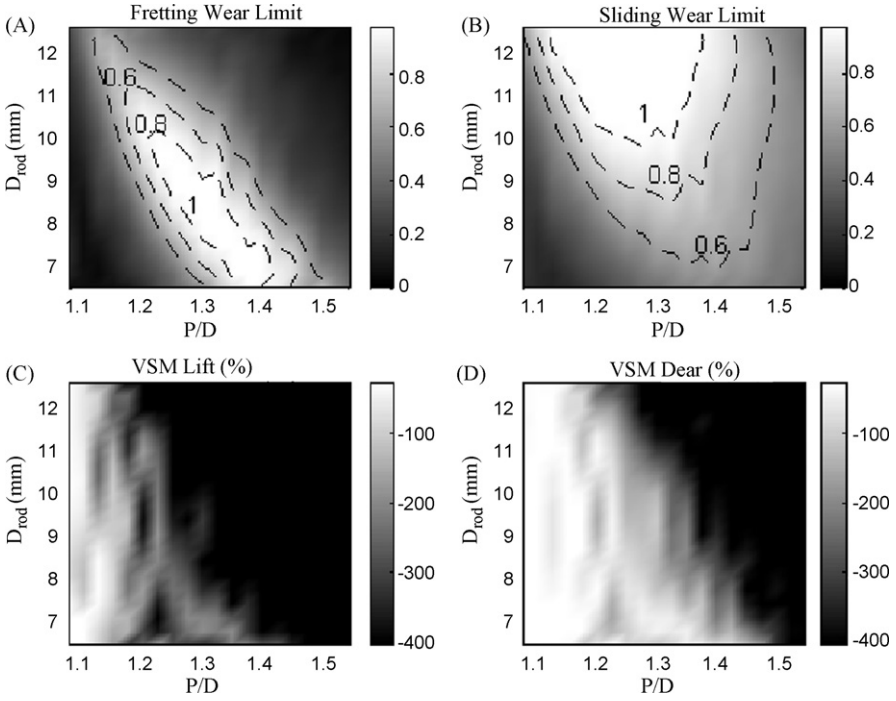

Fig. 12. Vibrations and wear constraints for 5% UO_2 at 0.414 MPa.

Please cite this article in press as: Shuffler, C., et al., Thermal hydraulic analysis for grid supported pressurized water reactor cores. Nucl. Eng. Des. (2009), doi:10.1016/j.nucengdes.2008.12.028

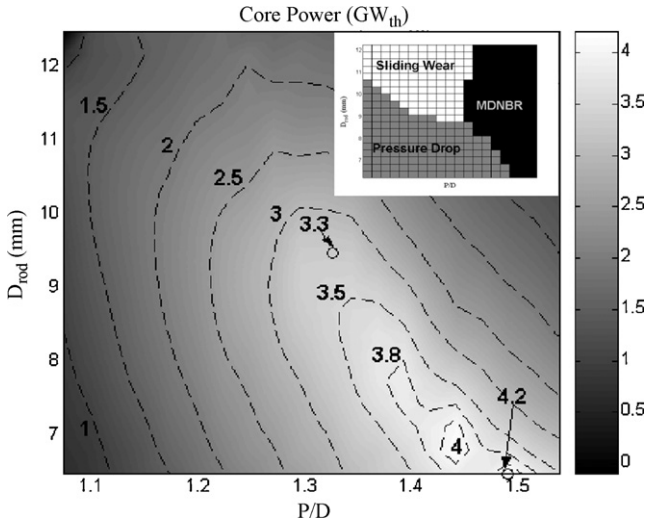

Fig. 13. Maximum power for 12.5% U–$ZrH_{1.6}$ incorporating steady-state and overpower transient design limits at 0.20 MPa.

and power for the new geometries to the reference core's rod number, average linear heat rate, and power. Fig. 14B shows that none of the new geometries yielded a higher average linear heat rate than the reference core after applying the steady-state and overpower transient design limits. The design constraints are plotted in Figs. 15 and 16.

The maximum power is 4.210 GW_{th}, or ~11% higher than the reference core power, and is achieved at the geometry: D_{rod} = 6.5 mm, P/D = 1.49. It is limited by the pressure drop constraint. A region exists inside of the reference power contour (i.e., 3.8 GW_{th}) in Fig. 13 indicating those designs which offer increased power relative to the reference PWR. In this region, the increased power results from increasing the number of fuel rods because the average linear heat rates are lower than the average linear heat rate for the reference PWR (See Fig. 14B). The power at the reference core geometry is 3.306 GW_{th}, or ~13% lower than the reference core power. The reason for this power reduction with hydride fuel is discussed in Section 6. MDNBR dominates as the most limiting constraint for larger P/D ratios. Pressure drop dominates for smaller rod diameters and P/D ratios, while sliding wear is the most limiting constraint for larger rod diameters and smaller P/D ratios. Fuel temperature, fluid-elastic instability, vortex shedding lock-in, fretting wear, and the overpower MDNBR do not constrain power for any geometries.

5.2.2. UO_2 results at 0.20 MPa

The maximum achievable power at the reference core pressure drop limit is presented in Fig. 17 for 5% enriched UO_2. Again, the power variations arise from changes in the average linear heat rate and rod number for each geometry relative to the reference PWR values. Fig. 18 plots the ratios of the rod number, average linear heat rate, and power for the new geometries to the reference core's rod number, average linear heat rate, and power. The design constraints are plotted in Figs. 19 and 20.

The maximum power is 4.168 GW_{th}, or ~10% higher than the reference core power, and is achieved at the geometry: D_{rod} = 6.82 mm, P/D = 1.44. Like the U–$ZrH_{1.6}$ case, it is limited by the pressure drop across the fuel bundle. A region exists inside of the reference power contour (i.e., 3.8 GW_{th}) in Fig. 17 indicating those designs which offer increased power relative to the reference PWR. Fig. 18 shows that these power gains are achieved by increasing the number of fuel rods in the core because no geometries offer a higher average linear heat rate than the reference PWR. The power at the reference core geometry is 3.8 GW_{th}, though it drops off substantially as the geometry changes slightly. This explains why the reference core geometry power in Fig. 17 is adjacent to the 3.5 GW_{th} contour. MDNBR dominates as the most limiting constraint for larger P/D ratios. Pressure drop dominates for smaller rod diameters and P/D ratios, while sliding wear is the most limiting constraint for larger rod diameters and P/D ratios between ~1.25 and 1.4.

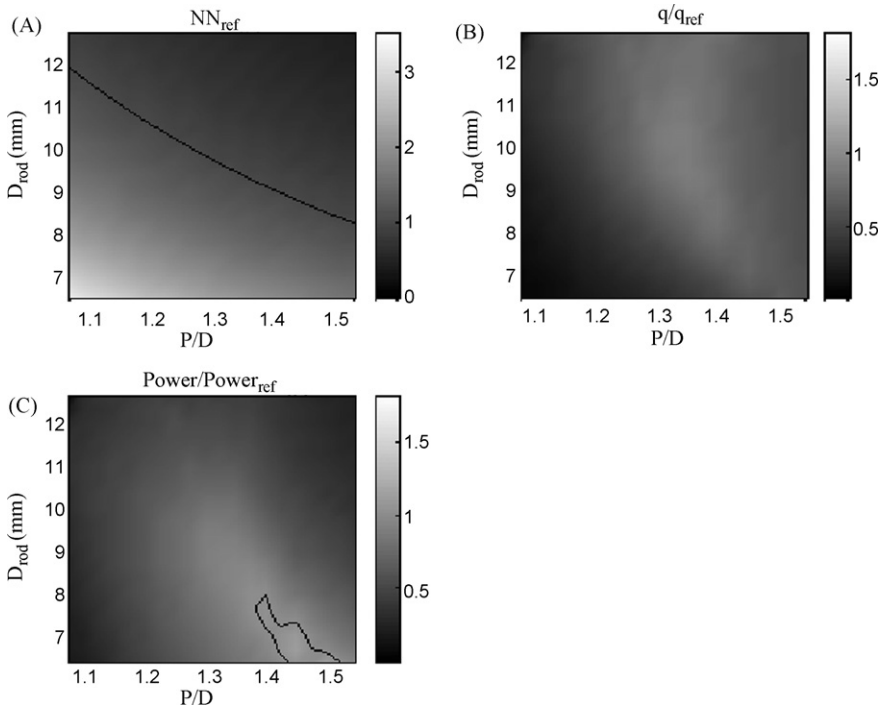

Fig. 14. Rod number, linear heat rate, and power ratios for 12.5% U–$ZrH_{1.6}$ at 0.20 MPa.

Please cite this article in press as: Shuffler, C., et al., Thermal hydraulic analysis for grid supported pressurized water reactor cores. Nucl. Eng. Des. (2009), doi:10.1016/j.nucengdes.2008.12.028

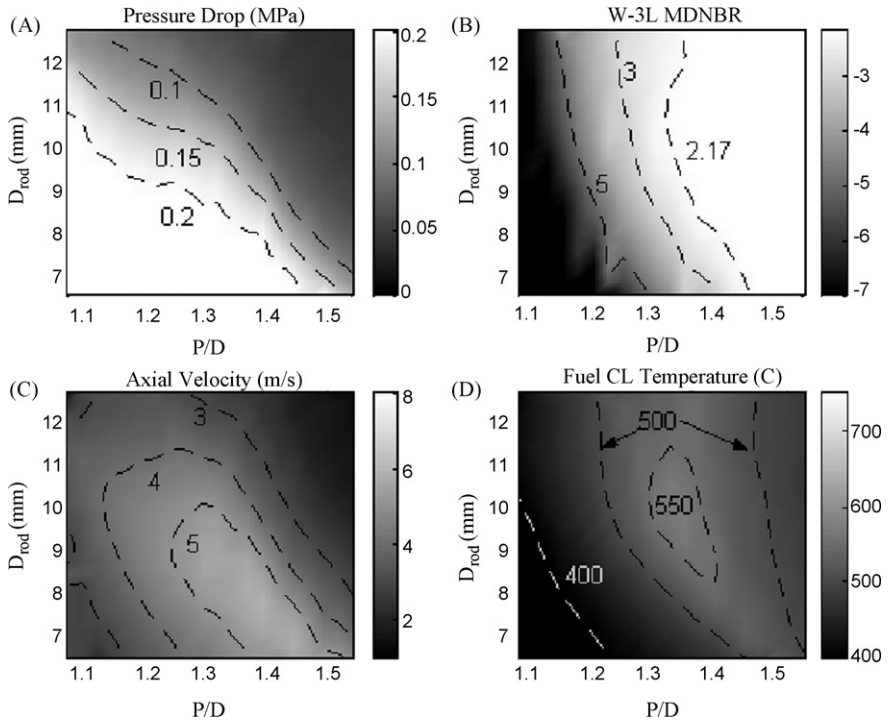

Fig. 15. Steady-state constraints for 12.5% U–$ZrH_{1.6}$ at 0.20 MPa.

5.3. *Maximum achievable power results (with LOCA)—hydride and oxide fuels*

As discussed in Section 4.3, the LOCA transient was not applied to all geometries in the parametric study. This section presents the results from application of the LOCA transient using the RELAP code for a single hydride and oxide fueled geometry. The geometry chosen is the peak power geometry from the steady-state analysis at the 0.414 MPa pressure drop limit. Though limited to a single geometry, this bounding LOCA calculation allows a qualitative estimate of the impact of the LOCA transient on the optimal geometries at the lower pressure drop limit.

Section 4.1 explained the basis for applying liquid metal bond to UO_2 fueled designs in the steady-state thermal hydraulic analysis with VIPRE. The LOCA calculation for the peak power UO_2 fueled design, however, incorporates helium fill in the gap to provide a

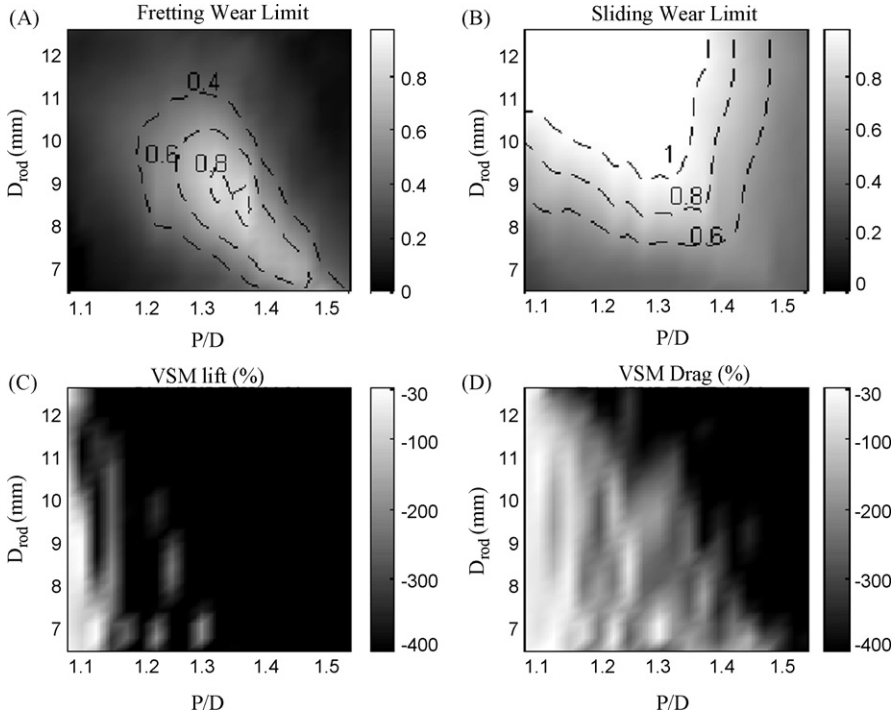

Fig. 16. Vibrations and wear constraints for 12.5% U–$ZrH_{1.6}$ at 0.20 MPa.

Please cite this article in press as: Shuffler, C., et al., Thermal hydraulic analysis for grid supported pressurized water reactor cores. Nucl. Eng. Des. (2009), doi:10.1016/j.nucengdes.2008.12.028

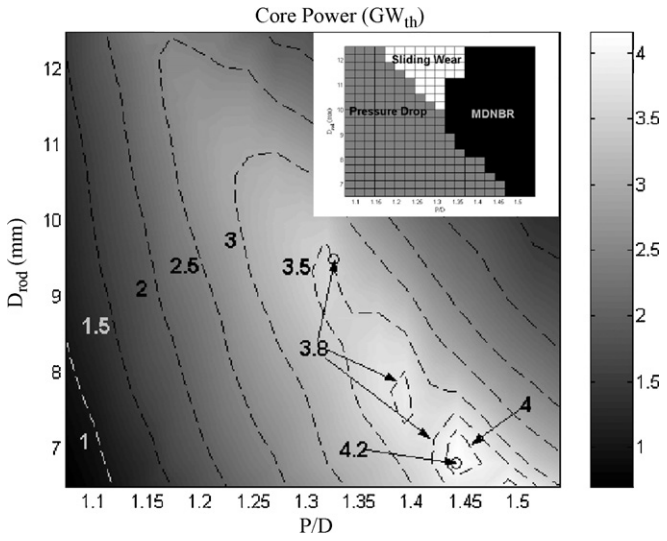

Fig. 17. Maximum power for 5% UO_2 incorporating steady-state and overpower transient design limits at 0.20 MPa.

more realistic estimate of fuel and cladding temperatures during the transient. Liquid metal fill properties were maintained for the U–$ZrH_{1.6}$ LOCA calculation.

Fig. 21 presents the time dependent peak U–$ZrH_{1.6}$ fuel temperatures for 5 axial zones when the LOCA transient is applied to the geometry D_{rod} = 6.5 mm, P/D = 1.39 operating at 5.016 GW_{th}. The maximum fuel temperature is 1165 K (892 °C), well below the 1050 °C temperature limit for the fuel. Due predominantly to the high thermal conductivity of U–$ZrH_{1.6}$ fuel and the small heat flux under decay heat conditions, the cladding temperatures (not plotted) are almost identical to the fuel temperature. The cladding temperatures were therefore much lower than their respective 1204 °C temperature limit.

The time dependent cladding temperature for UO_2 fuel is presented in Fig. 22 for the same geometry and power. The peak cladding temperature is ~1200 K (927 °C), well below the 1204 °C temperature limit for zircaloy established in 10CFR50.46. This is also well below the 1138 °C peak cladding temperature for the reference South Texas Project core presented in the plant's Final Safety Analysis Report (South Texas Project FSAR). The peak UO_2 fuel temperature (not plotted) is 960 °C, well below the 2800 °C temperature limit for the fuel.

The above analysis can be used to predict the transient performance of the peak power geometries for U–$ZrH_{1.6}$ and UO_2 fuels at the lower pressure drop limit. From Section 5.2, the steady-state peak power for U–$ZrH_{1.6}$ was 4.210 GW_{th} at the geometry: D_{rod} = 6.5 mm, P/D = 1.49. As compared to the U–$ZrH_{1.6}$ fueled design in Fig. 21, this design has both a lower steady-power before initiation of the transient and a larger pitch. It is therefore reasonable to conclude that the optimal 0.20 MPa design can be more easily quenched and will have lower fuel and cladding temperatures than the optimal 0.414 MPa design. The achievable power for the optimal U–$ZrH_{1.6}$ fueled steady-state geometry at the lower pressure drop limit will therefore not be affected by the LOCA transient. The same conclusion can be drawn for the peak power UO_2 fueled design at the lower pressure drop limit. From Section 5.2, its power is lower than design evaluated in Fig. 22, and its geometry is more open (i.e, pitch is larger). Further analysis with RELAP would evaluate the impact of the LOCA transient on the remainder of the design space. Such analysis was not considered necessary in this work since achievable power higher than the geometry discussed above is not expected to be achieved by alternate geometries.

5.4. Maximum achievable power results (with LOFA)—hydride and oxide fuels

As discussed in Section 4.3, complexities associated with the LOFA analysis prevented application of the LOFA transient to all geometries considered in the parametric study. As a result, the

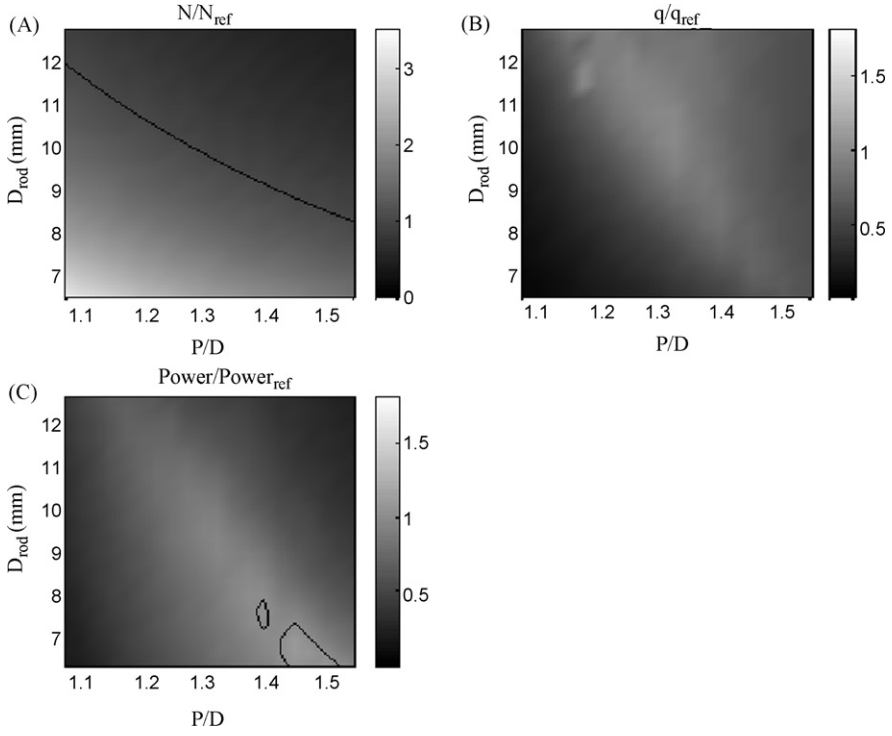

Fig. 18. Rod number, linear heat rate, and power ratios for 5% UO_2 at 0.20 MPa.

Please cite this article in press as: Shuffler, C., et al., Thermal hydraulic analysis for grid supported pressurized water reactor cores. Nucl. Eng. Des. (2009), doi:10.1016/j.nucengdes.2008.12.028

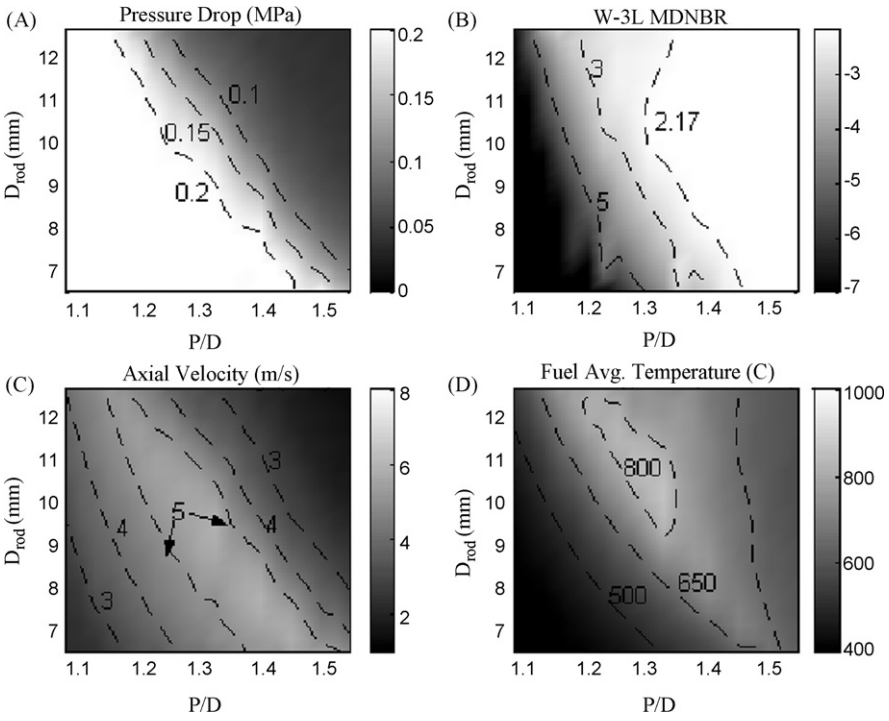

Fig. 19. Steady-state constraints for 5% UO_2 at 0.20 MPa.

LOFA transient was applied to two high power geometries for U–$ZrH_{1.6}$ and UO_2 fuels at the 0.414 MPa pressure drop limit identified in the steady-state analysis (i.e., the peak power geometries incorporating all design limits from Table 3). The results of this analysis are shown below. The peak power geometry (D_{rod} = 6.5 mm; P/D = 1.39 from Figs. 5 and 9) for U–$ZrH_{1.6}$ and UO_2 was reduced by ~200–4820 MW_{th}. The power reduction for another high power design with a similar geometry (D_{rod} = 6.82 mm; P/D = 1.37) was calculated as 53 MW_{th} for U–$ZrH_{1.6}$ and 204 MW_{th} for UO_2. These limited LOFA analyses suggest that the power reduction to accommodate the LOFA for the other designs subject to the 0.414 MPa pressure drop limit can be bounded by the 200 MW_{th} reduction calculated for the peak power geometry (Table 5).

The faster the rate of coastdown for new hydride and oxide designs relative the reference core, the more limiting the LOFA MDNBR is on power. The rate of coastdown depends on both the tightness of the pin array in the core and the mass flow rate at the start of the LOFA. Because the highest power geometries for

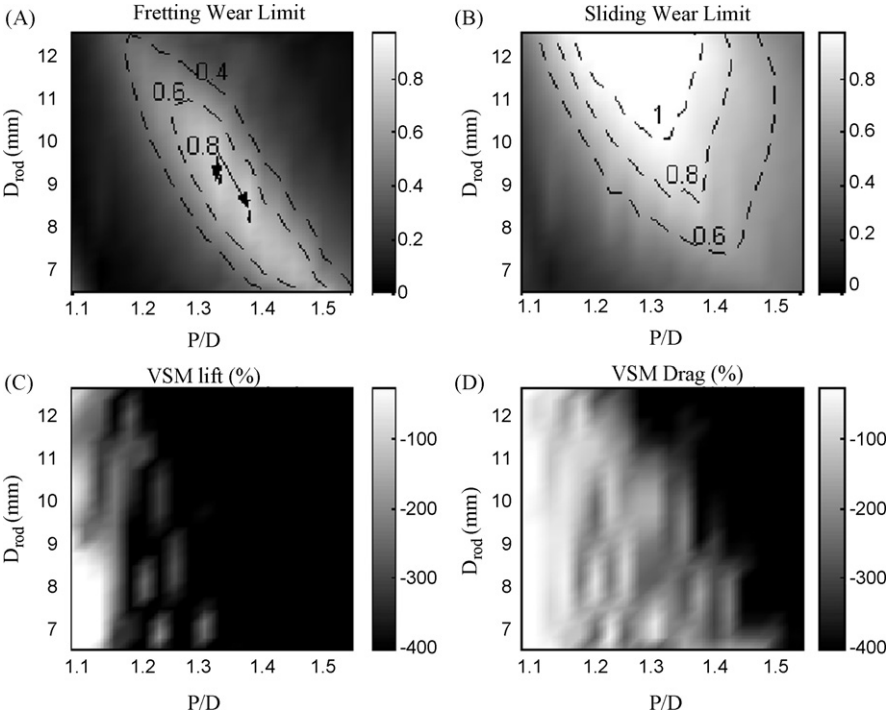

Fig. 20. Vibrations and wear constraints for 5% UO_2 at 0.20 MPa.

Please cite this article in press as: Shuffler, C., et al., Thermal hydraulic analysis for grid supported pressurized water reactor cores. Nucl. Eng. Des. (2009), doi:10.1016/j.nucengdes.2008.12.028

Table 5
LOFA results for 12.5% U–$ZrH_{1.6}$ and 5% UO_2 at 0.414 MPa.

P/D	D_{rod} (mm)	Power (MW_{th}) before LOFA (U–ZrH1.6)	Power (MW_{th}) before LOFA (UO2)	Power (MW_{th}) after LOFA
1.39	6.5	5016 (Fig. 5)	5000 (Fig. 9)	4820
1.37	6.82	4732 (Fig. 5)	4883 (Fig. 9)	4679

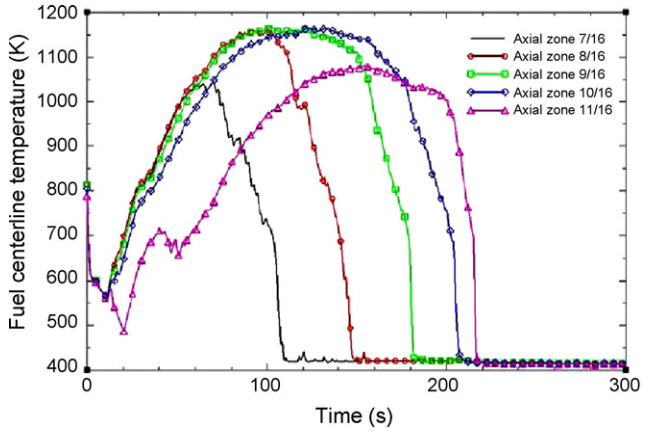

Fig. 21. Time dependent peak fuel temperature for the optimal U–$ZrH_{1.6}$ fueled design at 0.414 MPa.

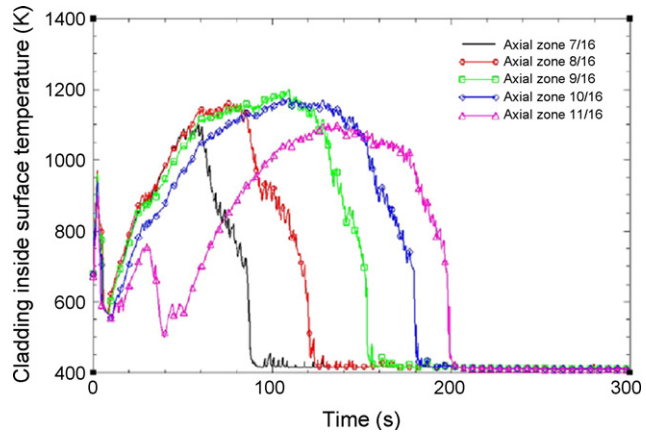

Fig. 22. Time dependent peak cladding temperature for the optimal UO_2 fueled design at 0.414 MPa.

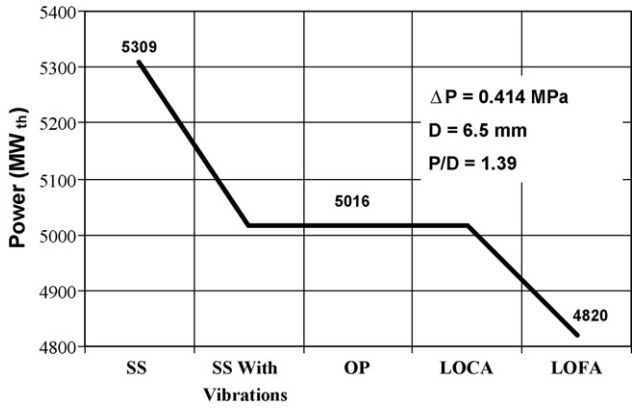

Fig. 23. Maximum power for 12.5% U–$ZrH_{1.6}$ at 0.414 MPa as a function of steady-state and transient design limits.

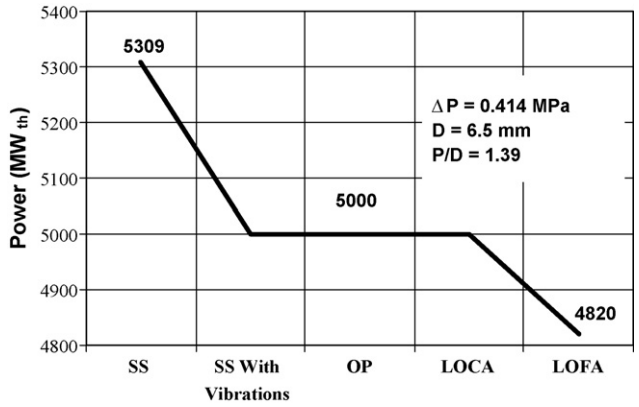

Fig. 24. Maximum power for 5% UO_2 at 0.414 MPa as a function of steady-state and transient design limits.

the 0.20 MPa pressure drop case have lower initial mass flow rates than at 0.414 MPa, and occur at looser configurations (i.e., larger P/D ratios), the LOFA is not expected to further reduce power. Consequently, Figs. 13 and 17 can be considered the final power maps for oxide and hydride fuels at the lower pressure drop limit including the LOFA constraint.

6. Final achievable power—hydride and oxide fuels

This thermal hydraulic analysis calculated the maximum achievable power for U–$ZrH_{1.6}$ and UO_2 fueled PWR cores as a function of steady-state, vibrations and wear, and transient design limits. Tables 6 and 7 summarize the peak power geometries and their respective thermal hydraulic operating parameters and limits. The last column in each table provides the corresponding operating information for the reference core.

The powers for the optimal geometries (i.e, $P/D = 1.39$, $D = 6.5$ mm) at the 0.414 MPa pressure drop limit for U–$ZrH_{1.6}$ and UO_2 are shown in Figs. 23 and 24 as a function of the applied thermal hydraulic design limits. The steady-state (SS) limits of MDNBR, fuel bundle pressure drop, and fuel temperature are initially applied. Vibrations and wear limits are then added, followed

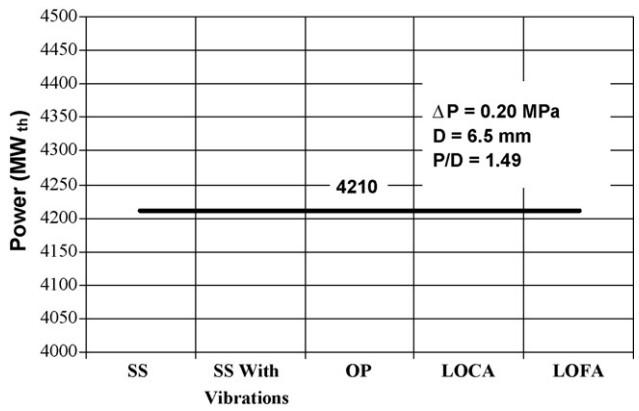

Fig. 25. Maximum power for 12.5% U–$ZrH_{1.6}$ at 0.20 MPa as a function of steady-state and transient design limits.

Please cite this article in press as: Shuffler, C., et al., Thermal hydraulic analysis for grid supported pressurized water reactor cores. Nucl. Eng. Des. (2009), doi:10.1016/j.nucengdes.2008.12.028

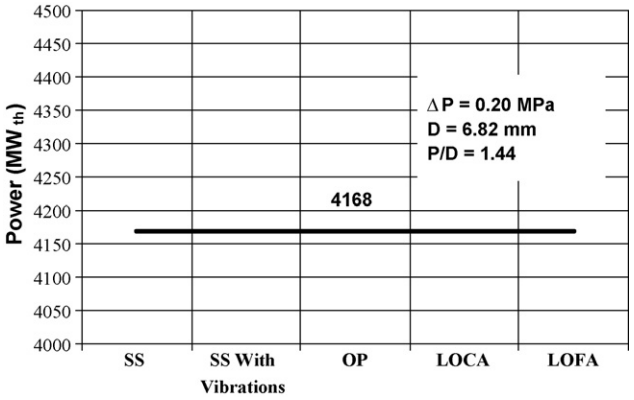

Fig. 26. Maximum power for 5% UO_2 at 0.20 MPa as a function of steady-state and transient design limits.

Table 6
Summary of maximum power results at 0.20 MPa.

Characteristic	0.20 MPa		Ref.
	U–$ZrH_{1.6}$	UO_2	
Power (MW_{th})	4210	4168	3800
D_{rod} (mm)	6.5	6.82	9.5
P/D	1.49	1.44	1.326
Number of fuel rods	86132	83758	52952
Avg. linear heat rate (kW/m)	11.45	11.65	17.52
MDNBR	2.19	2.40	2.17
Flow velocity* (m/s)	5.42	5.67	5.78
Fuel centerline temp (°C)	521.9		
Fuel average temp (°C)		656.3	872.7
Coolant mass flow rate (kg/s)	20635	20429	18627
Fuel bundle ΔP (MPa)	0.20	0.20	0.20
Limiting constraint	ΔP	ΔP	ΔP, MDNBR

* Average coolant velocity in the hot channel.

by the overpower (OP) transient, and the LOCA and LOFA events. For the 0.20 MPa pressure drop limit, the achievable power plots appear as flat lines, as shown in Figs. 25 and 26. Both of these designs are limited by the fuel bundle pressure drop limit. This occurs because the vibrations and transient limits did not limit the peak power geometries for U–$ZrH_{1.6}$ or UO_2. Further, as discussed in Sections 5.3 and 5.4, the LOCA and LOFA limits are not expected to further reduce the achievable power.

Comparing Figs. 5–9 and Figs. 13–17, it is observed that achievable power is slightly higher for UO_2 than U–$ZrH_{1.6}$ in regions limited by sliding and fretting wear. Understanding the reason for this requires an understanding of how the thermal hydraulic design limits are affected by the fuel type. MDNBR (steady-state and overpower), fuel bundle pressure drop, fluid-elastic instability, and vortex shedding lock-in are independent of the fuel type. The sliding and fretting wear limits, fuel temperature limit, and the LOCA limit are fuel dependent.

Table 7
Summary of maximum power results at 0.414 MPa.

Characteristic	0.414 MPa		Ref.
	U–$ZrH_{1.6}$	UO_2	
Power (MW_{th})	4820	4820	3800
D_{rod} (mm)	6.5	6.5	9.5
P/D	1.39	1.39	1.326
Number of fuel rods	98699	98699	52952
Linear heat rate (kW/m)	11.45	11.45	17.52
MDNBR	2.7	2.7	2.17
Flow velocity* (m/s)	7.08	7.08	5.78
Fuel centerline temp (°C)	518.5		
Fuel average temp (°C)		663.9	872.7
Coolant mass flow rate (kg/s)	23627	23627	18627
Fuel bundle ΔP (MPa)	0.34	0.34	0.20
Limiting constraint	LOFA	LOFA	ΔP, MDNBR

* Average coolant velocity in the hot channel.

The wear limits are fuel dependent because they are based on the time the fuel spends in the core. This was discussed in Section 3.1. U–$ZrH_{1.6}$ fuel, in general, offers higher energy generation per core loading than UO_2 (Ganda et al., 2009; Romano et al., 2009). The implication of this is that for the same power, U–$ZrH_{1.6}$ fuel will experience more rod wear. If the same cumulative rod wear limit is applied to both fuels, power must be reduced to a larger degree for the U–$ZrH_{1.6}$ design, to maintain its higher energy generation. A fundamental assumption in the wear analysis is that power is the only design variable considered to impact the vibrations and wear performance of new designs (See the Appendix). A design with either fuel type that exceeds the wear limit can be made acceptable, however, by other means. Examples include increasing the number of grid spacers, increasing the cladding thickness, or reducing the discharge burnup in the fuel. Choosing burnup as the design variable would have enabled higher powers to be achieved in both UO_2 and U–$ZrH_{1.6}$ designs limited by either sliding or fretting wear. In fact, the two power maps would be almost identical, with an exception for geometries limited by the other fuel dependent constraints (i.e., fuel temperature, LOCA). There may be a trade off, however, in the economic attractiveness of these designs, as reduced burnup will increase the fuel cycle costs (though increasing power will work to offset this). An economic optimization study could therefore be performed to derive the best approach for applying the vibrations and wear limits (i.e., changing burnup versus power), though this was not attempted with this study.

7. Conclusions

A parametric study was undertaken to determine the maximum achievable power that can be safely sustained in U–$ZrH_{1.6}$ and UO_2 fueled PWR cores constructed of traditional square array fuel assemblies with grid spacers. Steady-state and transient design limits were applied including MDNBR (for steady-state, LOFA, and an overpower transient), fuel bundle pressure drop, fuel temperature (steady-state), fluid-elastic instability margin, vortex shedding margin, cumulative sliding and fretting wear, and fuel and cladding temperatures (LOCA). The major conclusions of this study are as follows:

1) In spite of the relatively low permissible operating temperature of hydride fuel, the peak power attainable using hydride fuel is comparable to that attainable with oxide fuel. In other words, the hydride fuel temperature limit does not constrain the power attainable with hydride fuel.
2) As a result of the low steady-state fuel temperature combined with the relatively low stored energy in hydride fuel, the cladding and fuel temperatures during a LOCA are lower for hydride fueled designs relative to oxide fueled designs.
3) Significant power gains can be realized for U–$ZrH_{1.6}$ and UO_2 fuels at both pressure drop limits compared to the reference core power output of 3800 MW_{th}. These gains are achieved at geometries that differ from the reference core design. Peak gains compared to the reference PWR are ~400 MW_{th} (~10%) at the 0.20 MPa pressure drop limit, and over 1000 MW_{th} (~27%) at the 0.414 MPa pressure drop limit. The peak powers for U–$ZrH_{1.6}$ are 4.210 GW_{th} and 4.820 GW_{th} at pressure drop limits of 0.20 and 0.414 MPa. These peak powers occur at the geometries D = 6.5 mm, P/D = 1.49, and D = 6.5 mm, P/D = 1.39, respectively. The peak powers for UO_2 are 4.168 GW_{th} and 4.820 GW_{th} at pressure drop limits of 0.20 and 0.414 MPa. These peak powers

Please cite this article in press as: Shuffler, C., et al., Thermal hydraulic analysis for grid supported pressurized water reactor cores. Nucl. Eng. Des. (2009), doi:10.1016/j.nucengdes.2008.12.028

occur at the geometries $D = 6.82$ mm, $P/D = 1.44$, and $D = 6.5$ mm, $P/D = 1.39$ respectively.

In addition, large design regions exist at both pressure drop limits for U–$ZrH_{1.6}$ and UO_2 fuels where power gains can be achieved relative to the reference core. These geometries, in general, have smaller rod diameters and larger P/D ratios than the reference core geometry (i.e, $D = 9.5$ mm, $P/D = 1.326$). This analysis showed that the gains are obtained by increasing the number of fuel rods in the reactor vessel; none of the higher power designs have a larger average linear heat rate than the reference core.

4) The thermal hydraulic performance of U–$ZrH_{1.6}$ and UO_2 fuels is very similar. The primary reason for this conclusion is that the fuel dependent design limits (steady-state fuel temperature, fretting wear, sliding wear, and LOCA cladding and fuel temperatures) are generally not as restrictive on power and constrain fewer geometries than the limits that are independent of fuel properties (steady-state MDNBR, LOFA MDNBR, and fuel bundle pressure drop). Differences in achievable power do exist, however, when fuel dependent design constraints are most limiting, notably in fretting and sliding wear limited regions. The power differences in these regions could be eliminated by applying the wear constraints in a different manner. This paper limited the cumulative fretting and sliding wear for new designs to that of the reference core. Wear is the product of wear rate, which depends on power, and the time the fuel spends in the core, which depends on power, burnup, and heavy metal inventory. This work reduced power whenever wear limits were exceeded. Alternately, burnup could be reduced to shorten the time spent by fuel in the core to enable operation at a higher power. This second approach to applying the wear limits would essentially eliminate wear as a limiting constraint on power. The power maps for U–$ZrH_{1.6}$ and UO_2 would therefore be almost identical, with a few exceptions for geometries limited by the other fuel dependent constraints (i.e., steady-state fuel temperature, LOCA cladding and fuel temperatures). There may be a trade off, however, in the economic attractiveness of these designs, as reduced burnup will increase the fuel cycle costs. Increasing power will work to offset this, and so further optimization is required to determine the most effective approach for applying the wear limits.

Nomenclature

A_{cl}	cladding cross-sectional area
A_o	outer rod cross sectional area
A_{surf}	fuel rod outer surface area
c_p	fuel constant pressure specific heat
D	rod outer diameter
D_{clad}	mean cladding diameter
$D_{core\text{-}perp}$	core dimension perpendicular to the fuel assemblies
$D_{core\text{-}diag}$	core dimension cut diagonally across the fuel assemblies
D_{gap}	mean gap diameter
D_h	hydraulic rod diameter
D_{ref}	reference PWR rod diameter
D_{rod}	rod outer diameter
E_{cl}	cladding Young's modulus
FIM	fluid-elastic instability margin
f_n	nth natural frequency of the rod
f_s	vortex shedding frequency
f_1	fundamental rod frequency
F_n	normal contact force between the rod and support spring
$F_{q'}$	radial peak to average power ratio
$F_{q'axial}$	axial peak to average power ratio
g	diametral gap between the tube and support
G_F	random force power spectral density
Δh	core enthalpy rise
$\bar{h}$	average coolant heat transfer coefficient
h_{cool}	coolant heat transfer coefficient
h_{gap}	gap heat transfer coefficient
I_{cl}	cladding moment of inertia
J_{11}	joint acceptance
k_{clad}	cladding thermal conductivity
k_{fuel}	fuel thermal conductivity
K	5.0 for turbulent flow
K_{rod}	rod wear coefficient (material dependent)
l_{assm}	fuel assembly length (i.e., sides)
L	fuel rod length
$L_{assembly}$	fuel assembly length (i.e., height)
L_h	active fuel rod length
L_s	average length between spacers
m_t	total linear mass of the fuel rod
n	number of rods per assembly
n_s	number of spans (between grid spacers)
N_{grid}	number of grid spacers
P	pitch
P/D	pitch to diameter ratio
$(P/D)_{ref}$	reference PWR pitch to diameter ratio
ΔP	pressure drop across the fuel bundle
P_o	steady-state operating power
P_{sat}	primary system pressure
q'	linear heat rate
Q	cumulative volume of material removed by wear
$Q_{fretting}$	cumulative volume of material removed by fretting wear
Q_{new}	cumulative wear for a new design
Q_{ref}	cumulative wear for the reference core
$Q_{sliding}$	cumulative volume of material removed by sliding wear
$\dot{Q}$	power
$\dot{Q}_{ref}$	reference PWR power
R_{core}	core radius
Re	Reynold's number
S	Strouhal number
S_d	total sliding distance
t	time
t_{clad}	cladding thickness
t_g	gap thickness
t_{grid}	grid spacer thickness
$t_{MCT,BD}$	time to minimum cladding temperature during blowdown
$t_{PCT,BD}$	time to peak cladding temperature during blowdown
$T_{average}$	fuel average temperature
$T_{centerline}$	fuel centerline temperature
T_{cool}	coolant temperature at the axial location of the peak cladding temperature
T_c	cycle length
$T_{c,new}$	cycle length for a new design
$T_{c,ref}$	cycle length for the reference core
$T_{clad,inl}$	initial cladding temperature
T_{inlet}	core inlet coolant temperature
$T_{PCT,BD}$	peak cladding temperature during blowdown
T_{peak}	peak temperature
$\bar{T}_S$	average coolant saturation temperature
$T(t)_{clad}$	time dependent cladding temperature
V	fuel volume
V_{axial}	peak axial velocity
$V_{critical}$	critical cross-flow velocity
V_{cross}	cross-flow velocity
V_{eff}	effective cross-flow velocity
VSM_{drag}	vortex shedding margin in the drag direction
VSM_{lift}	vortex shedding margin in the lift direction
$\dot{W}_{fretting}$	fretting wear rate
$\dot{W}_{sliding}$	sliding wear rate

Please cite this article in press as: Shuffler, C., et al., Thermal hydraulic analysis for grid supported pressurized water reactor cores. Nucl. Eng. Des. (2009), doi:10.1016/j.nucengdes.2008.12.028

x	coolant subchannel axial position
y_{rms}	total root mean square rod response
$y_{rms\text{-}axial}$	axial-flow root mean square rod response
$y_{rms\text{-}cross}$	cross-flow root mean square rod response
α	π for simply supported rods
ρ	fuel density
ρ_{fl}	coolant density
μ	coefficient of friction
ζ	damping ratio
ζ_1	first mode damping ratio
$\psi_1(x)$	rod first mode shape function

Appendix A

The equations supporting the vibrations and wear analysis in this Appendix are derived from Au-Yang (2001).

A.1. Vibrations and wear analysis assumptions

The following simplifying assumptions were made so that the vibrations analysis can be performed without the aid of advanced computational tools and with best-practice guidance in the academic literature:

- *The fuel rod is modeled as a linear structure*: This assumption is based on treating the grid supports as single pin supports. In reality, the gapped support condition between the grid spacer and the fuel rod allows relative movement between the two components. With this movement, non-linear finite element analysis (FEA) codes are needed to quantitatively model the rod response, which is beyond the scope of this work. A linear rod model and experimental correlations for rod response are used as a substitute.
- *Changes to the fuel assembly structure over time are not considered:* Core operating conditions play a significant role in the structural mechanics of fuel assembly components during fuel irradiation. For example, creep-down of the cladding due to pressure forces, support spring relaxation due to irradiation, and wear accumulation combine to slowly open the gap between the fuel rod and its support. Oxidation from temperature extremes and irradiation change the material properties of all structural components in the core. Rod bow may also occur, changing the rod/support structure interaction and the flow distribution of coolant in the core. Because of the difficulty associated with modeling these effects, and the lack of guidance outside of proprietary vendor computer codes, structural changes to the rod and support structure are neglected.
- *Only the cladding structure is considered in the fuel rod model:* A gap exists for fresh fuel rods between the fuel pellets and the cladding. Over time, the fuel swells closing this gap, and it contacts the cladding surface. In addition, gases generated by the fission process and any burnable absorbers present pressurize the pin. For conservatism, the additional rigidity provided by fuel swelling and rod pressurization is not considered.
- *Only the first vibration mode is considered:* The first vibration mode (fundamental mode) typically has the largest impact on rod vibration. With regard to vortex shedding lock-in and fluid-elastic instability, the use of the first mode typically yields the most conservative design margin. Furthermore, several correlations used in place of FEA codes for modeling turbulence-induced vibration response are only applicable for the fundamental mode.

An additional assumption involves the selection of design parameters that enable new core designs to comply with vibrations and wear design limits. For a fixed geometry, the thermal hydraulic limits discussed in Section 3.1 are strictly functions of core power (i.e., new designs that exceed these limits can only be made acceptable by reducing power). The vibrations and wear analysis, however, has additional variables which can potentially be modified to meet the applicable design criteria. For example, a core design that fails the fluid-elastic instability criteria can be made acceptable by reducing power, increasing the number of grid spacers, or increasing cladding thickness. Designs that fail the wear criteria can be made acceptable by reducing power which reduces coolant flow and rod vibration or reducing the discharge burnup in the fuel, which reduces the length of time the fuel is susceptible to wear. For this analysis, power is the only design variable considered to impact the vibrations and wear performance of new designs. Note that this has a significant impact on the final thermal hydraulic results in regions limited by fretting and sliding wear, as discussed in Section 6.

A.2. Derivation of effective and critical velocities

The cross-flow velocity is not uniform across a fuel rod. The effective cross-flow velocity provides a solution for this by weighting the cross-flow velocity profile over the rod by the vibration mode shape of the rod. Cross-flows occurring at the mid-point between grid spacers, where the vibration amplitude is largest, will therefore be given more weight than cross-flows occurring at the supports, where the amplitudes are approximately zero. Neglecting changes in the coolant density and linear mass axially along the gap, the effective cross-flow velocity for the first mode is given by

$$V_{eff} = \sqrt{\frac{\int_0^{L_t} V_{cross}^2(x)\psi_1^2(x)\,dx}{\int_0^{L_t} \psi_1^2(x)\,dx}} \tag{A.1}$$

where, $\psi_1^2(x)$: rod first mode shape function; x: coolant subchannel axial position

The most widely accepted correlation for estimating the critical velocity for a tube bundle is Connor's equation:

$$V_{critical} = \beta f_n \sqrt{\frac{2\pi\zeta m_t}{\rho_{fl}}} \tag{A.2}$$

where, f_n: nth natural frequency of the rod; ζ: damping ratio; m_t: total linear mass of the fuel rod; ρ_{fl}: coolant density

Pettigrew suggested a P/D effect on Connors' constant:

$$\beta = 4.76\left(\frac{P}{D} - 1\right) + 0.76 \tag{A.3}$$

The critical velocity is constant for a fixed geometry and, with the exception of small changes in coolant density, does not depend on the power and flow conditions in the core. Evident in Connor's equation is the conservatism accompanying the use of the first natural frequency, which yields the lowest critical velocity and the largest FIM. Because of the relationship between effective cross-flow velocity and power, the FIM will scale with power and can therefore be incorporated as a design constraint into the thermal hydraulic analysis.

A.3. Derivation of root mean square rod response

The upper bound RMS rod response from turbulent cross-flow is given by

$$y_{rms\text{-}cross} = \sqrt{\frac{2n_s G_F}{64\pi^3 m_t^2 f_1^3 \zeta} J_{11}} \tag{A.4}$$

where, n_s: number of spans (between grid spacers); G_F: random force power spectral density; J_{11}: joint acceptance

G_F in Eq. (A.4) is a function of the cross-flow velocity in the core. For conservatism, the peak cross-flow velocity determined by VIPRE

Please cite this article in press as: Shuffler, C., et al., Thermal hydraulic analysis for grid supported pressurized water reactor cores. Nucl. Eng. Des. (2009), doi:10.1016/j.nucengdes.2008.12.028

is used in the calculation of the rod response. The upper bound RMS rod response from axial-flow turbulence is

$$y_{\text{max-axial}} = \frac{1}{3}5E - 5DK\alpha^{-4}\left(\frac{u^{1.6}\varepsilon^{1.8}Re^{0.25}}{1+u^2}\right)\left(\frac{D_h}{D}\right)^{0.4}\left(\frac{\beta^{0.67}}{1+4\beta}\right) \tag{A.5}$$

where

$$u : V_{\text{axial}}L_s\sqrt{\frac{\rho_{fl}A_o}{E_{cl}I_{cl}}} \tag{A.6}$$

A_o: outer rod cross sectional area; D_h: hydraulic diameter; L_s: average length between spacers; Re: Reynold's number; V_{axial}: peak axial velocity; α: π for simply supported rods; β: $\rho_{fl}(A_o/m_t)$; ε: L_s/D; K: 5.0 for turbulent flowAgain, for conservatism, the axial velocity input to Eq. (A.6) was the maximum axial velocity determined by VIPRE. The total RMS rod response is equal to the sum of the cross and axial flow contributions:

$$y_{\text{rms}} = y_{\text{rms-axial}} + y_{\text{rms-cross}} \tag{A.7}$$

A.4. Derivation of the sliding and fretting wear limit equations

A.4.1. Fretting wear

Yetisir et al. suggested that the fretting wear rate can be approximated as the power dissipated by the vibrating rod. The power dissipation depends on the structural properties of the rod and the RMS response from flow-induced vibration (i.e., as given by Eq. (A.7)). The power dissipation, or fretting wear rate, for the first vibration mode is given by

$$\dot{W}_{\text{fretting}} = 32\pi^3\zeta_1 f_1^3 L_s m_t y_{\text{rms}}^2 \tag{A.8}$$

The cumulative volume of material removed by fretting wear, Q_{fretting}, is the product of the fretting wear rate, time, t, and a material dependent wear coefficient:

$$Q_{\text{fretting}} = \dot{W}_{\text{fretting}}K_{\text{rod}}t \tag{A.9}$$

where, K_{rod}: wear coefficient (material dependent)

The ratio of the cumulative fretting wear in new hydride or oxide fueled geometries to the cumulative fretting wear in the reference core must remain below unity. Recognizing that the damping ratio, length between grid spacers, and wear coefficient are the same for new geometries and the reference core, the cumulative fretting wear ratio can be written as

$$\frac{Q_{\text{fretting,new}}}{Q_{\text{fretting,ref}}} = \frac{\dot{W}_{\text{fretting,new}}}{\dot{W}_{\text{fretting,ref}}}\frac{T_{c,\text{new}}}{T_{c,\text{ref}}} = \frac{(f_1^3 m_t y_{\text{rms}}^2)_{\text{new}}}{(f_1^3 m_t y_{\text{rms}}^2)_{\text{ref}}}\frac{T_{c,\text{new}}}{T_{c,\text{ref}}} \le 1 \tag{A.10}$$

A.4.2. Sliding wear

Connors suggested that the sliding wear rate is equal to the product of the normal contact force between the rod and support spring, F_n, and the differential change in the total sliding distance, S_d, with respect to time.

$$\dot{W}_{sliding} = F_n \cdot \frac{dS_d}{dt} \tag{A.11}$$

The normal contact force is given by

$$F_n = \frac{3\pi D y_{\text{rms}}}{\mu((L_s/A_{cl}E_{cl}) + (D^2L_s^2/4E_{cl}I_{cl}))} \tag{A.12}$$

where A_{cl}: cladding cross-sectional area; E_{cl}: cladding Young's Modulus; I_{cl}: cladding moment of inertia; μ: coefficient of friction

The sliding distance is given by

$$S_d = \pi f_1 g t \tag{A.13}$$

where, g: diametral gap between the tube and support

The cumulative sliding wear at time t is obtained by substituting Eqs. (A.12) and (A.13) into Eq. (A.11), and substituting this result into Eq. (A.9). The result, as shown below, is known as Archard's equation:

$$Q_{\text{sliding}} = \dot{W}_{\text{fretting}}K_{\text{rod}}t = \pi K_{\text{rod}}F_n f_1 g t \tag{A.14}$$

As in the case of fretting wear, the cumulative sliding wear in new designs is limited to the cumulative sliding wear in the reference core. The cumulative sliding wear ratio must again be less than or equal to one:

$$\frac{Q_{\text{sliding,new}}}{Q_{\text{sliding,ref}}} = \frac{\dot{W}_{\text{sliding,new}}T_{c,\text{new}}}{\dot{W}_{\text{sliding,ref}}T_{c,\text{ref}}} = \frac{(Dy_{\text{rms}}f_1)_{\text{new}}((1/A_{cl}) + (D^2/4I_{cl}))_{\text{ref}}T_{c,\text{new}}}{(Dy_{\text{rms}}f_1)_{\text{ref}}((1/A_{cl}) + (D^2/4I_{cl}))_{\text{new}}T_{c,\text{ref}}} \le 1 \tag{A.15}$$

References

Au-Yang, M.K., 2001. Flow-Induced Vibration of Power and Process Plant Components. ASME Press, New York. pp. 62, 141, 149, 166–167, 181, 259, 265–267, 308, 359.

Ganda, F., Greenspan, E., Petrovic, B., 2009. Reactor physics analysis for PWR cores. Nucl. Eng. Des., doi:10.1016/j.nucengdes.2008.12.027.

Garkisch, H., Petrovic, B., 2003 (March). Reference Data and Constraints for Uranium–Zirconium-Hydride and Uranium–Thorium Hydride Fuels for Light Water Reactors. Westinghouse Electric Company LLC.

Malen, J., Todreas, N., Romano A., 2004 (March). Thermal hydraulic design of hydride fueled pwr cores. MIT-NFC-TR-062, MIT, Center for Advanced Nuclear Energy Systems.

Olander, D., Garkisch, H., Petrovic, B., Greenspan, E., 2009. Hydride fuel materials performance and design constraints. Nucl. Eng. Des., doi:10.1016/j.nucengdes.2009.04.001.

Romano, A., Shuffler, C., Garkisch, H., Olander, D., Todreas, N., 2009. Fuel Performance Analysis for PWR Cores. Nucl. Eng. Des., doi:10.1016/j.nucengdes.2008.11.022.

Shuffler, C., Trant, J., Todreas, N., Romano, A., 2006 (September). Thermal hydraulic and economic analysis of grid-supported hydride and oxide fueled PWRs, MIT-NFC-TR-077, MIT, Center for Advanced Nuclear Energy Systems.

Shuffler, C., Diller, P., Todreas, N., Greenspan, E., Petrovic, B., 2009. Economic analysis of grid and wire wrap supported hydride and oxide fueled PWRs. Nucl. Eng. Des., doi:10.1016/j.nucengdes.2009.01.017.

South Texas Project Electric Generating Station Final Safety Analysis Report, Revision 12.

Stewart, C., 1989 (August). VIPRE-01: a thermal hydraulic code for reactor cores. Volume II User's Manual.

Please cite this article in press as: Shuffler, C., et al., Thermal hydraulic analysis for grid supported pressurized water reactor cores. Nucl. Eng. Des. (2009), doi:10.1016/j.nucengdes.2008.12.028